USING VIRTUAL FRACTURE REDUCTION SOFTWARE TO EXPLORE FEATURES FOR FRACTURE SEVERITY PREDICTION

by

Rewa S. Tikekar

A thesis submitted to the faculty of
The University of North Carolina at Charlotte
in partial fulfillment of the requirements
for the degree of Master of Science in
Electrical Engineering

Charlotte

2015

Approved by:

_____
Dr. Andrew Willis

_____
Dr. Thomas Weldon

_____
Dr. James Conrad

ABSTRACT

REWA S. TIKEKAR. Using virtual fracture reduction software to explore features for fracture severity prediction. (Under the direction of DR. ANDREW WILLIS)

Current medical treatment for comminuted bone fractures, i.e., traumatic bone fractures that result in many bone fragments, is based upon fracture severity classifications that physicians determine subjectively. Due to the subjectivity in the interpretation of the available information, the severity of a single fracture case may be classified differently by physicians. Accurate, reliable, and repeatable classification of fracture severity is an important factor in planning effective treatment and an overall positive prognosis for difficult fracture cases. Recent work has placed an emphasis on developing computational tools to analyze CT image data and estimate fracture severity.This research explores the statistical relationships between fracture severity and quantities derived from a new virtual bone fracture reconstruction system. Many of these quantities have not been previously available due to the lack of a system capable of virtually reconstructing highly-fragmented bone fractures. The existence of a new bone reconstruction system makes available a new set of measurable values whose relationships to fracture severity have been discussed but never been quantitatively examined. The relation between fracture severity and these quantities is heretofore unknown and this thesis provides an initial analysis of utility of these features for fracture severity prediction via automated CT image analysis. This thesis discusses the predictive capabilities of features for fracture severity for seven clinical cases, ranked by three orthopaedic surgeons.

ACKNOWLEDGEMENTS

I would like to thank my advisor, Dr. Andrew Willis, for his constant support and guidance. I am extremely grateful for the unmatched academic experience which I gained under his guidance.

I also thank my parents, my sister and my family for being a constant source of support. Living away from home was not as easy as perceived earlier, and I cannot imagine all this time without numerous international calls and Skype conversations. I am grateful to their effort, to try their best to be there for me, across oceans.

TABLE OF CONTENTS

LIST OF FIGURES

LIST OF TABLES

CHAPTER 1: INTRODUCTION

Quantifying fracture severity for highly comminuted fractures is a challenging task and is widely studied throughout the orthopaedic trauma literature [1, 2]. Research in [3] states that accurately assessing fracture severity for a highly comminuted bone fracture is a key factor in determining joint health. Having identified the significance of fracture severity assessment for treatment, many researchers [4, 5, 6] have explored computational approaches that seek to estimate fracture severity from image measurements. Approaches extract features from the image data automatically or semi-automatically , and values of these features are used to infer severity. Inferencing methods typically exploit correlations between the extracted feature values and limb trauma to predict the fracture severity. As a benchmark fracture severity values provided by practicing physicians are used to evaluate the utility of a feature for severity prediction. This thesis refers to these computationally-extracted features as *fracture features* and investigates the utility of a number of novel fracture features for their utility in predicting fracture severity.

1.1 Problem Statement

As noted in [7], fracture severity prediction places itself as the single most important factor in predicting the long term affects of a highly comminuted bone fracture. The primary approach for fracture severity assessment is to approximate the severity from visual observations of the injury and CT imagery. However, fracture severity is difficult to evaluate by visual assessment for complex, multi-fragment fractures, especially at joint locations. This is evident by the variability observed in fracture severity ratings assigned by physicians for a complex fracture cases. Recent work

seeks to analyze medical image data to predict fracture severity and potentially help reduce variability now present. This thesis investigates five different fracture features from medical image data and provides an initial characterization of their utility for predicting fracture severity. The analyzed bone fracture features are divided into three distinct categories:

- Geometric features (2),
- Tissue related features (1),
- Mechanical features (2).

Fracture features are computed using a virtual fracture reconstruction system that reconstructs unbroken bone and extract fracture features from the virtual bone fragments . This system makes available a quantitative values for a number of heretofore unexplored fracture features and this thesis explores several of these new features. Statistical evaluation of their predictive performance provides new information regarding the relative importance of these quantities for predicting fracture severity.

1.2 Motivation

Fracture severity classification is an important aspect of fracture treatment [4]. It helps physicians to diagnose and plan treatment, establish a notion of the risk of complications and allows one to estimate fracture recovery time. Fracture severity is also useful for indicating whether a fracture will lead to Post Traumatic Osteo-Arthritis(PTOA) [8]. Fracture measures help physicians to treat new cases by studying fracture treatment patterns obtained from prior cases. Because fracture classification plays an important role in fracture treatment and long term joint health, accurately determining the fracture severity of a fracture becomes a crucial step in fracture diagnosis. Fracture severity is often subjectively determined by one or more physicians which can be subject to bias due to variability in each physician's background and experience. In complex and highly traumatic fractures it is possible that

this variability in severity classification may lead to a treatment plan that is not "best practice." Fracture severity classification from CT image data can provide unbiased estimates of fracture severity estimation [6] as they are based on computationally-derived fracture measures extracted from medical image data. As such, it becomes important to explore and evaluate quantitative approaches for fracture severity classification which may help build consensus and improve accuracy in difficult fracture classification contexts.

1.3 Outline Of Approach

This thesis uses 3D CT images of the fractured limb and a virtual reconstruction system to reconstruct the unbroken bone. Where appropriate, new functions were added to the reconstruction system software to extract the analyzed fracture severity features. The analysis approach used extracts five different features from 3D CT images of seven clinical fracture cases and analyzes the utility of these features for the purpose of predicting the severity of the fracture. The performance of each feature is measured by a goodness-of-fit measure that correlates values of the extracted features with quantitative severity measures assigned to each case by by three orthopaedic surgeons. Different models for this correlation are explored including a linear regression model. Those features found to minimize the error between the feature values and the surgeon-assigned values are deemed to be the best predictors of fracture severity.

1.4 Goal And Contribution

This thesis provides the first comparative analysis of the predictive power of several important features thought to be strongly linked to fracture severity. The features capture distinct aspects of the fracture event and are categorized into three areas: (1) geometric features and (2) tissue features, and (3) mechanical features. The comparative analysis allows researchers to better understand the links between these features and fracture severity as well as the inter-relationships between these features.

In addition, some of the bone fracture features analyzed in this thesis have not been previously evaluated. This is attributed to the lack of a system capable of virtually reconstructing highly fragmented bone fractures which is integral to the analysis methods of this thesis. The existence of this new bone reconstruction system makes it possible to extract quantitative values for these features.

CHAPTER 2: BACKGROUND INFORMATION AND FEATURE SELECTION

This chapter discusses background information needed to understand our fracture analysis approach. It explains the nature of the recorded CT image data, the novel algorithms and technologies applied and provides descriptions of the clinical context of the study which focuses on severe traumatic fractures of the tibia at the ankle joint.

This thesis relies on the technologies developed in [9], which conceived a system for virtually reconstructing bone fractures from 3D CT images of the fractured limb. This system takes 3D CT images of a fracture case as input and outputs a virtual 3D model of the reconstructed unbroken bone. The system accomplishes this task in a series of three steps:

1. The system segments the CT images [10] to extract 3D models of the bone fragments.

2. Each bone fragment is then partitioned into anatomic regions to allow their surfaces to be matched during reconstruction.

3. A virtual reconstruction of the unbroken bone is computed by applying a puzzle-solving algorithm on the anatomically partitioned fragments.

Using the reconstruction result, a number of features that have been suspected to be good predictors of fracture severity assesmentcan be directly extracted. These are:

- Number of fragments.

- Bone density information for each fragment.

- 3D models for bone sub-surfaces by anatomic region.

- Location for fragments with respect to each other and their geometric relationship to the original unbroken bone.

This thesis describes methods to extract these fracture features and analyzes the performance of these features for predicting fracture severity.

This thesis specifically focuses on tibial plafond fractures as shown in Figure 2.2 [6]. These fractures most commonly result from high energy trauma such as that caused by vehicular accidents or falls from heights. Tibial plafond fractures are an important sub-class of fracture cases. Accurate prediction of fracture severity is important for this sub-class for the following reasons:

- Due to their complex structure, these fractures are difficult to treat and are more susceptible to fracture severity mis-classification.
- These fractures form a significant population of all traumatic fracture cases and effective treatment can significantly impact long-term limb function [7].

The assessment of fracture severity prediction performance in this thesis contributes directly to state-of-art in image-based fracture analysis.

This thesis is structured as follows: Chapter 1 introduces the problem of fracture severity prediction and states the motivation and goal that drives this research. Chapter 2 elaborates on the background information leading to the fracture feature selected for analysis and their specific definitions. It also describes medical image data terminologies and bone feature properties as they relate to the goals of this thesis. Chapter 3 discusses the virtual bone reconstruction system and related previous work. Chapter 4 describes the methodologies used to extract fracture features from medical image data. Chapter 5 provides the feature extraction results and an analysis of the measured feature values for seven clinical fracture cases. Chapter 6 and 7 discusses the case results, and analyzes the statistical information derived from

case-wise analysis. It also compares the quantitative feature value results with the observations made by orthopaedic surgeons.

Terminology:

Some terminology used throughout this write-up are defined here to simplify the discussion. In this thesis, we denote the 3D CT image obtained from patient's fractured limb as the fracture CT image, and the 3D CT image obtained from the patient's healthy limb as the intact CT image. We denote the outer surface of bone excluding articular surface as the periosteal surface, the smooth surfaces at the end of bones used for joint movement are articular surface, and the fracture surface of a bone are the surfaces generated when the bone broke apart. Finally, we denote unbroken bone surface extracted from the intact CT image as the intact template, and the bone fragment surfaces extracted from the fracture CT image as bone fragments.

2.1 Background Information

2.1.1 Medical Imaging

Medical imaging technologies capture measurements from the tissues of the body represented by a collection of positions (usually a 2D or 3D grid) which is then viewed as a digital image. The images are used as data to conduct bone fracture analysis. Imaging tools are helpful for diagnosis of bone abnormalities and for fracture treatment planning.

Bone images are an important source of quantitative data for bone fracture analysis. As noted in [11, 12], the visual assessment of severity by physicians can widely disagree on grading fracture condition. Highly comminuted bone fractures are more difficult to diagnose without the aid of imagery and can have more significant disparity in severity from visual assessment. Multiple imaging modalities can facilitate analysis by providing different views of a particular bone region. These varying modalities can help explore image data for new fracture predicting features [10].

2.1.2 Medical Imaging Modality

Computed Tomography (CT) is a powerful medical imaging modality for producing 2-D and 3-D images of tissues within the body using X-ray. CT scans are particularly useful for bone tissue analysis because they provide a sharper image for bone tissue than other modalities. As such, important characteristics of a bone such as the dimension, shape, internal structure and density can be readily extracted from CT images via automatic methods.

2.1.3 File Formats: The PLY Format And The DICOM Medical Image Format

This thesis makes use of 3D medical image and surface data to compute fracture features. PLY is a 3D model file format designed to represent three dimensional surfaces. The PLY file format is used to store representations of the geometry of the fragment surfaces and key surface attributes including: color and transparency.

The Digital Imaging and Communications in Medicine (DICOM) standard is typically used to store image information from medical sensor devices, e.g., 3D CT. In the case of 3D CT machines, the DICOM images appear as a stack of 2D gray scale images which helps to view a bone in three dimension. The gray scale value of each pixel is an indication of the x-ray attenuation coefficient for the material occurring at the pixel location. This thesis uses the gray scale intensity values stored in DICOM images to extract structural bone information, e.g., bone fragments surfaces, at fracture locations which subsequently facilitate fracture severity estimation.

A detailed account of DICOM data structure, header format and various network oriented services for information transfer is given in [13]. Certain open source applications are used to read and understand DICOM images so that relevant information can be extracted [14]. It is established to facilitate secure image information exchange over the network, between medical imaging equipment and other systems [15]. Pixel intensity information is extracted from DICOM in order to compute tissue related

severity feature.

2.1.4 Hounsfield Intensity

A HU is a 2D or 3D unit used to describe gray scale intensity value at a pixel location. A CT image consists of array of x-ray data commonly converted to standardized Hounsfield Units (HU) so that the images generated from different CT imaging machines can be put into a format having a single characterization of tissues by their intensity. Cancellous bone (spongy bone) tissue typically has a substantially lower Hounsfield intensity than cortical bone (dense bone) tissue. We derive the Hounsfield intensity by following conversion

$$H = I(m + \alpha) \tag{2.1}$$

where, H denotes the Hounsfield intensity, I is pixel intensity, m denotes slope (as indicated in DICOM header (ex: tag 0028, 1053)) and α is $y - axis$ intercept (as indicated in DICOM header (ex: tag 0028, 1052)). The Hounsfield intensity is used in this thesis as effective way to normalize CT intensities, which are machine-dependent, to a common physically-based intensity scale. This provides a more robust values for processing the measured bone density information in a bone fracture and helps in identifying anatomic location of that fracture [16].

2.1.5 The Intact Template And The Contra-lateral Limb

The virtual reconstruction system uses a 3D model of the unbroken bone as a template into which the 3D bone fragments are fit during reconstruction. This model is defined as the intact template and is estimated from a 3D CT image of the contra-lateral limb. In this way the image of the contra-lateral limb serves as a reference shape into which the broken fragments can be fit for reconstruction. The scans of the intact contra-lateral limb also serves as an approximation of the fractured limb prior to the fracture event. This study requires a scan of the intact contra-lateral virtual reconstruction methods. Further, the reconstruction assumes that the intact

anatomy of the fractured limb is well approximated by its limb's lateral counter part.

2.1.6 Ankle Joint

The ankle joint is a complex joint, formed by the connection of three bones. The top of the talus (ankle bone) fits inside a socket that is formed by the lower end of the tibia (shinbone) and the fibula (the small bone of the lower leg) shown in Figure 2.1. The ankle joint permits two movements: i) Plantar flexion (flexion), in which the foot is pointed downwards (normal range of motion is: 20-50°) ii) Dorsiflexion (extension), in which the foot is raised (normal range motion: 10-30°) [17].

Such movements are possible due to the presence of cartilage [18], a connective tissue, which facilitates a smooth motion of joints. The cartilage lining is about one-quarter of an inch thick in most joints that carry body weight. It is soft to withstand a shock but tough to last a lifetime. The thickness and the volume of the cartilage is determined by genetic factors [19]. Ankle joints are more prone to post fracture inflammation due to thin cartilage lining. All the cases studied in this thesis are traumatic fractures of the ankle joint.

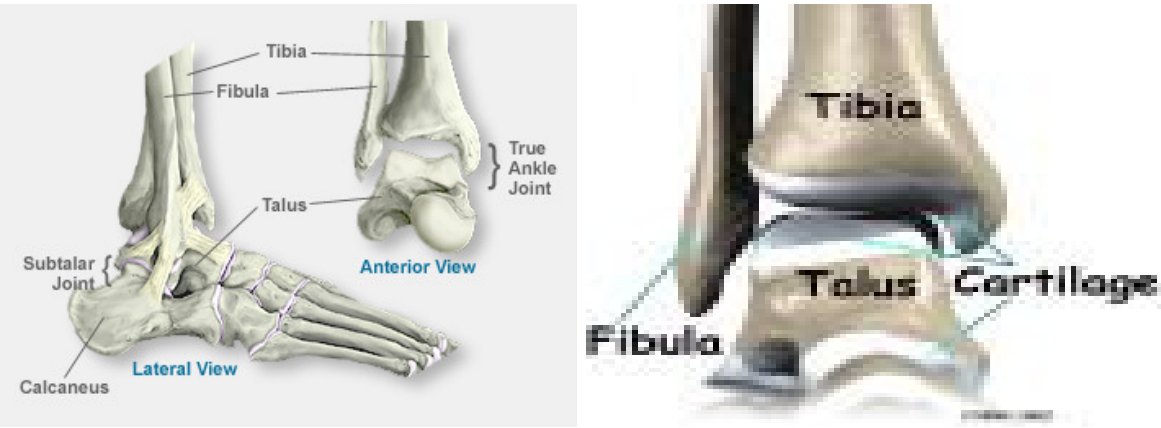

(a) Ankle joint (b) Cartilage

Figure 2.1: Anatomy of the ankle showing thecartilage of the joint.

2.1.7 Bone Fracture, Tibial Plafond Fracture Classification And Their Treatment

A fracture occurs when a bone fails to withstand some force and breaks. A tibial plafond fracture occurs when the fracture involves the tibia and the ankle joint. Because there is little muscle and skin surrounding the ankle joint, tibial plafond fractures are problematic. Tibial plafond fractures occur when extreme axial and/or rotational forces are imparted to the bone causing varying degrees of displacement, articular comminution (breaking of the joint articulating surface) and metaphyseal disruption (breaking of the bone). Such axial and rotational forces cause translational and angular displacement of the fracture fragments which are the two fracture features analyzed in this thesis.

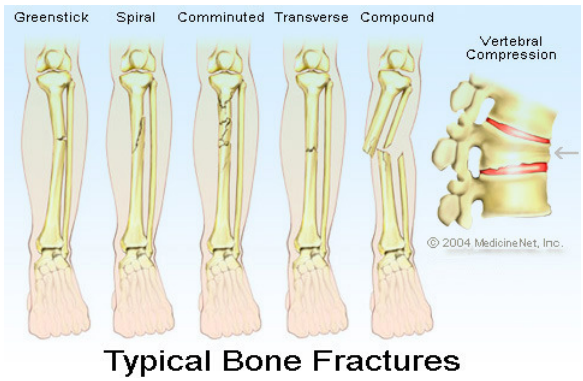

Figure 2.2: Few typical bone fractures [20]

If the soft-tissues around the fracture are too swollen and damaged, surgery may not be possible. In such cases, surgery may be delayed until the swelling subsides and the soft-tissue condition improves. Proper fracture treatment procedures must be followed to expedite the healing process [21, 6]. Following are the types of tibial plafond fractures and their respective optimal recommended treatment strategies.

Table 2.1: Tibial plafond fractures and their treatment

Severity classification	Condition	Treatment
1	Simple fracture, no articular displacement.	Closed treatment methods
2	Presence of articular displacement, less metaphyseal disruption	Rigid internal fixation (fix by using screws, metal plates)
3	Large metaphyseal disruption	Rigid internal fixation method
4	Large metaphyseal disruption, less articular comminution	Rigid internal fixation method
5	Large articular comminution	Rigid internal fixation

Rigid internal fixation has shown better results in treating type 3, 4, 5 fractures. The clinical cases used in this thesis to explore fracture severity measures are tibial plafond fractures of ankle joint.

2.1.8 Post Traumatic Osteo Arthritis (PTOA)

PTOA is a condition caused by inflammation of a joint after an injury. Knee, ankle, hip, spine and hand joints are susceptible to inflammation and PTOA [22]. Clinical studies show that mechanical forces, intra-articular fractures and joint dislocation are some of the causes for joint failures [5, 23]. Progressive joint degeneration caused by bone fractures lead to Post Traumatic Osteo Arthritis (PTOA) [8]. Joint degradation is an irreversible, slow and continuous process which can affect any joint in the body. Degradation cause irreparable cartilage damage and painful joint function [24].

Recent research has explored the links between fracture severity and PTOA [25, 26]. PTOA's serious health condition which leads to substantial pain, disability, loss of

work and decreased general health status. Its overall adverse impact on an individual's physical and psychological well-being is comparable to that of other major disorders such as stroke, heart disease or diabetes [27]. The societal cost of PTOA is high (estimated at $12 billion/year in the U.S.), since pain and loss of function frequently leads to loss of work capacity [28, 29]. In order to reduce the possibility of PTOA, certain treatment guidelines were researched to achieve ankle stability and reducing the post-surgery joint incongruities [30].

2.2 Feature Selection

2.2.1 Bone Fracture Mechanics

Bone fracture mechanics is the study of how cracks are created and propagated in a bone. For several decades, fracture mechanics principles have been utilized to examine various aspects of bone failure [31, 32]. The theory of fracture mechanics states that there is a direct relation between the energy absorbed by the fracture and surface area liberated (surface area generated upon fracture event). Further, the energy absorbed is also theoretically linked to the area of the generated bone fragment fracture surfaces. The sum of these areas is referred to as the liberated surface area for a fracture. Experienced clinicians generally relate injuries with large numbers of fragments to "high energy" accidents. To understand this relationship quantitatively, this thesis includes analysis of the fragment fracture surface area to better understand the linkages between this feature and fracture severity.

2.2.2 Bone Material Properties

Bones, though light-weight, are hard and strong. They provide rigidity to the body structure. Bone composition is complex and dependent on various cell interactions and mineral deposition [33]. The two primary types of bones are i) cancellous bone and ii) cortical bone. The cortical bone tissue tends to have a lamellar structure acting as a dense outer shell (porosity- measure of void space: 5% to 30%). The can-

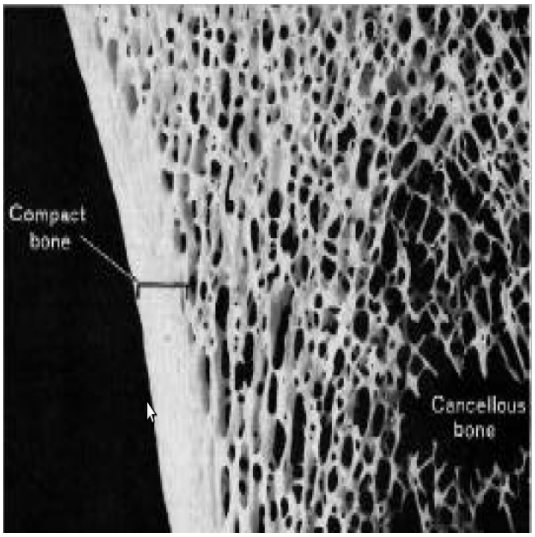

Figure 2.3: Cancellous and compact (cortical) bone tissue [36]

cellous bone, i.e, spongy bone, is similar to a three dimensional honey-comb structure (porosity: 30% to 90%). Bone tissue density varies depending on biological, dietary and habitual factors. Fracture severity measures are material-dependent, and are known to vary with bone density [34, 35]. CT images capture measurements of bone tissue density throughout the body [16]. This thesis includes a method to compute a feature that considers the density of the tissues separated when the bone tissue was broken into fragments, referred to as a tissue feature. This feature is based on the image intensities observed at the bone fragment fracture surface locations and its utility for fracture severity analysis is investigated.

2.2.3 Bone Strength And Micro-fracturing

A single or repetitive load through daily activities affects the bone structure and results in micro-fractures. Repetitive loading occurs in many activities, but most notably it is a characteristic of walking, running, and most other sports activities. The lamellar organization of the cortical bone prevents micro-fractures from migrating to interior structure. Excessive micro-fracture causes transverse and longitudinal crack formations which disrupt bone structure. Though being contained, these micro-fractures decrease bone strength and the bone may fracture at much lower loads than

it would have normally required [31, 37]. These micro-fractures pave way for larger fracture surfaces, i.e., surfaces generated when bone breaks apart [34, 32, 35]. This thesis analyzes fracture surface area and fracture surface perimeter as mechanical indicators of fracture severity.

2.2.4 Bone Surface Segmentation

Bone surface segmentation is the process of partitioning a 3D surface model of a bone into surface patches such that each patch is semantically distinct, i.e, different anatomically or by shape [38, 39, 40, 41, 42]. Bone surface segmentation sub-divides the bone fragment models into parts which enable analysis of important bone fragment sub-structures, e.g, the fragment fracture surface. Segmentation methods should be accurate, reproducible and robust to ensure efficient working of reconstruction algorithms and accurate values for the computed fracture surface area and fracture surface perimeter features. This thesis uses region growing and ridge walking segmentation algorithms to segment 3D bone models described as follows:

Ridge walking algorithm: This surface segmentation algorithm results in number of regions by computing boundaries that follow concave and convex valley like structures within a geometric model [43]. Applications of this segmentation method include surface compression and object recognition.

Region growing algorithm: Region growing is a simple pixel-based segmentation algorithm. The surface patches are generated based on predefined classification factor like color [44]. Given an image or a group of pixels, number of regions are formed which include the pixels that satisfy the predefined classification criteria. This method has wide range of application in image segmentation, video segmentation and comparison of fMRI activation detection [45].

Above mentioned algorithms are instrumental in generating fracture surfaces that are used as basis for running methods over to compute fracture features.

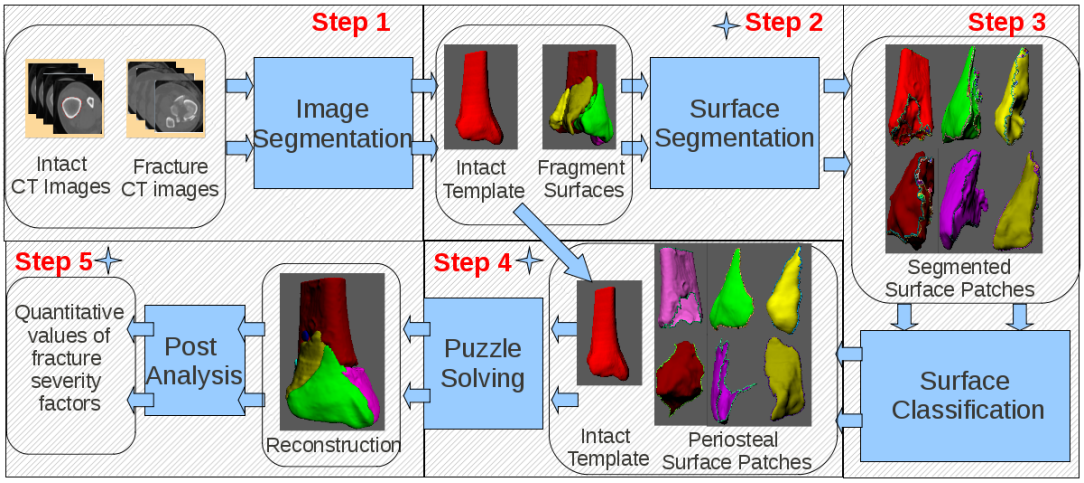

Figure 2.4: A brief overview of 3D reconstruction system which takes fracture CT images and intact CT images as input and provides a virtual reconstruction of bone fragments which estimates the anatomy of patient's original bone. Solid color denotes the process by which the data has been changed to allow for a reconstruction to be computed.

2.2.5 3D Reconstruction Process

Reconstruction can be defined as a process of classifying fracture surfaces and putting the fracture surface and fragment boundaries back together. Early efforts toward computer-aided bone fracture reconstruction include a system for reconstructing a simple two-fragment bone fracture [46, 47]. Interactive approaches for bone fragment alignment and reconstruction have since been proposed in [48] and in [49]. [48] emphasizes development of a realistic bone reconstruction system that performs real-time collision detection to prevent fragment collision. In [49], the authors describe an interactive system to reconstruct a 5-fragment comminuted bone fracture, which relies on manual interaction to position the bone [50][51]. Work in [16] describes an automatic system capable of reconstructing bone fractures. [52] talks about improving inter-fragmentary alignment for virtual 3D reconstruction of highly comminuted bones. This virtual reconstruction method is used in this thesis to reconstruct the unbroken bone 2.4.

As described in Figure 2.4, virtual reconstruction of the bone fragments can be

described in five following steps:

1. Fragment surfaces are extracted from CT images.

2. Each fragment surface is then further decomposed into sub-regions.

3. The surfaces are classified into anatomically meaningful patches.

4. Fragment patches are pieced back together in a virtual space with a puzzle-solving algorithm.

5. Post analysis on reconstructed fracture helps to assess the severity of the bone fracture.

This thesis elaborates on post analysis and explores various means to explore fracture features. Fracture measures are investigated by fusing geometry and function, at all steps of reconstruction process. Reliability of fracture feature value depends on the accuracy of fragment segmentation and fracture reconstruction.

CHAPTER 3: LITERATURE REVIEW

3.1 Fracture Severity And Related Features

Various attempts have been made to define computational methods that compute fracture measures. These approaches use medical images of fractured bone as source data for their computational approach [1, 6]. These approaches draw inspiration from the key factors indicated by physicians to be indicative of fracture severity. These key factors are:

- fragment displacement,
- fragment angular dislocation,
- number and size of fragments,
- soft tissue damage/skin disruption,
- location of fracture in bone.

where higher values for these measures suggests higher fracture severity.

Currently, many visually based classification systems are based on the fracture location in the bone (part of the bone), number of fragments (simple/multi-fragmentary), skin disruption (open/close) [2], anatomic description and orientation of fracture (transverse, spiral, oblique) [53, 54, 20]. This thesis uses two visually-assessed fracture severity values from 3 different orthopedic surgeons:

1. A quantitative severity score (0-100).
2. Kellgren-Lawrence (KL) grading scheme: is one of the oldest radiographic fracture severity classification systems which is used widely to classify fractures [55].

It classifies fracture severity to one of the five grades (0 - 4). Each grade (0 - 4) corresponds to increasing likelihood of PTOA (referred simply as OA) where the indications are (0) no OA, (1) doubtful OA, (2) minimal OA, (3) moderate OA and (4) severe OA respectively [56].

The fracture cases discussed in this thesis are also classified according to AO/OTA classification as depicted in Figure 3.1. This classification is not used for analysis but it does provide an additional indication of the extent of the severity of each discussed fracture case.

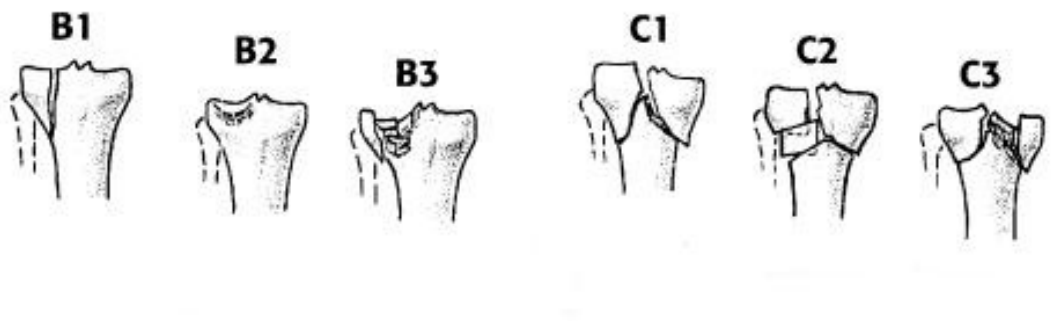

Figure 3.1: Broad AO/OTA classification for tibial plateau fractures: B1, split fractures only; B2, depressed fractures only; B3, combined split and depression; C1, articular simple, metaphyseal simple; C2, articular simple, metaphyseal multi fragmentary; and C3, multi fragmentary articular.

3.2 Fragment Convex Hull: Displaced Soft Tissue Volume

In this research the authors detect the bone fragments in a CT image of afractured limb and use the volume of the convex hull, i.e., volume encompassed by the smallest convex envelope that includes the bone surfaces, to predict fracture severity. Severity is computed by taking the difference in volume of the fracture convex hull previously described and the convex hull of the intact bone obtained by a CT of the (presumed intact) contralateral limb [2]. The authors found that higher volume differences is an indicator of increased fracture severity [39].

CHAPTER 4: METHODOLOGY

This chapter discusses the methods used to compute the fracture features and assess their performance. Towards this end, the chapter includes discussions of the clinical data collected for analysis the definition of the fracture features computed and the techniques applied to measure the performance of the fracture features for fracture severity prediction.

4.1 Clinical Data Collection And Assessment

Clinical data used for the analysis of this thesis consists of patient data gathered from seven clinical cases. The cases for this study range from low energy fracture events such as 1.5 foot fall, to high energy fracture events such as speeding crashes (80 mph), and includes a population having relatively younger patients (mean age 35 years). The focus of this research is tibial plafond fractures, which are obtained from a set of patients enrolled in an NIH-funded grant that sponsors this research. The enrollment criteria require patients to be less than 65 years of age and to be free of presence of osteo-arthritis. The pool of plafond fractures included in this study varies from simple articular fractures to highly comminuted and displaced fractures. The selection of patients was done by an experienced orthopedic surgeon and effort has been made to include a wide range of fracture variation.

Most of the injuries underwent a visual analysis performed by a set of orthopedic surgeons based on CT scans and radiographs. In some cases, emergency measures were taken to cater to severe dislocation after which a CT scan was taken. This clinical study has seven of such fractures, which are OTA Figure 3.1 classified as follows:

Table 4.1: Patient demographic and acute injury information for the rank 7 ordered cases. MVA: Moving vehicular accident; ATV: All terrain vehicle accident.

Case#	Sex	Age	OTA X ray Classification	Injury mechanism
6	F	38	C32	MVA (50mph)
7	M	21	B13	Fall (30 ft)
8	F	42	C21	MVA (30mph)
9	M	20	C13	ATV
10	M	24	C23	Fall (12 ft)
11	M	34	C11	Fall (18 ft)
12	M	29	B12	ATV

With repeated imaging studies collected from patients over the span of two years, PTOA was assessed on weight bearing radiographs using KL grading scale. All the seven cases were assigned overall severity score ranging from (1-100) by three orthopaedic surgeons (C1, C2, C3), KL scores and binary OA status by three surgeons after studying radiographs Table 4.2. This grading was based on number of factors like the number of fragments, size of fragments, displacement of the fragments, soft tissue damage and articular damage.

Table 4.2: Kellgren-Lawrence (KL) scores for 7 cases (5 grades; 0 – no OA, 4 – severe OA), binary OA status (1-OA; 0 - no OA) and overall severity (1-100) listing.

Case#	KL score	Binary OA status	Overall Severity			
			C1	C2	C3	Savg
6	2	1	60	55	60	58
7	4	1	50	60	58	56
8	4	1	62	80	79	74
9	0	0	6	15	32	18
10	3	1	55	57	62	59
11	4	1	70	65	77	71
12	0	0	5	27	10	14

There is a general agreement between the ranking schemes with almost 90% ac-

cordance between clinical observations. The fracture severity measures discussed in this thesis are measured against average overall severity score and KL score. There is about 60% correlation between those two ranking schemes for the cases under study. Binary OA status is mentioned flagging the possibility of OA.

4.2 Fracture Feature Computation

Fracture features are computed as a function of the bone fragment segmentation and from the virtual fracture reconstruction result. The bone fragment segmentation results provides the spatial locations where bone tissues broke apart due to the fracture event. As such, the CT intensities observed at the segmented bone fragment surface locations indicate both the types of tissues separated during the fracture event and how much of these tissues were torn apart in this process. For this reason, features derived from the bone fragment segmentation result are referred to as tissue and mechanical fracture features. The reconstruction tool provides estimates for the geometric transformations needed to move and orient each bone fragment from its location in the fractured CT to its anatomic location within the unbroken bone. For this reason, features derived from the virtual fracture reconstruction tool are referred to as geometric features. The specific fracture features analyzed in this thesis, and their respective categories, are listed below:

1. Geometric features:
   (a) Translational displacement,
   (b) Orientation displacement.
2. Tissue related feature:
   (a) Skewness of fracture intensity histogram.
3. Mechanical features:

(a) Fracture surface area,

(b) Fracture surface perimeter.

The following sections provide formal definitions for each of these features and describe the method/algorithm used to compute their values.

4.2.1 Geometric Features (Translational And Orientation Measure)

The bone fragment displacements provided by the virtual fracture reconstruction result measure how much the fragment position and orientation changed due to the fracture event. Non-anatomic motion of the bone fragments necessarily tear and displace soft tissues and, as a result, these measures can also be perceived as an approximate measure of soft tissue rupture and disruption. Due to these reasons, the dislocation of a bone fragment from its normal anatomic position is considered as a fracture measure.

Every fracture fragment follows a certain path, depending on the force of fracture event, and upsets the integrity of the adjoining region. This displacement can be measured as a combination of translational and rotational motion of fragments in a fracture case. High energy fractures result in ruptures of the intact bone that cause bone fragments to separate and disperse out of the initially intact bone composite structure. This results in soft tissue wounds and localized damage. A precise depiction of the shift is possible if a comparison is done between the intact, i.e., anatomic, and fracture position of the fragment. The process of reconstruction involves moving the bone fragments in a way similar that used to solve a 3D jigsaw puzzle. Here, correspondences between the bone fragments in their fractured position and their aligned/anatomic position provides an estimate of a plausible trajectory for the fragment in terms of angular and translational motion. As shown in Figure 4.2b, the change in centroid $\|C_1 - C_2\|$ of the fragment as described in § 4.2.1.1 and the change in angle of orientation [4.2.1.2] are computed from the reconstructed fracture. These

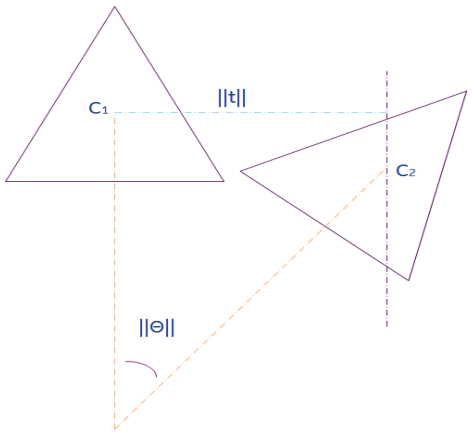

Figure 4.1: Illustration of the geometric interpretation of the translational and angular displacement features

provide measures of angular ($\|\theta\|$) and translational ($\|t\|$) displacement, respectively

where, C_1 is centroid of original object in space; C_2 is the centroid of the displaced object in space; $\|\theta\|$ is angular displacement and $\|t\|$ is translational displacement.

4.2.1.1 Centroid

In 3D geometry, the centroid C is defined as the center of mass for the object. For 3D models, the centriod is taken as the virtual center of mass given by assigning equal weight to each 3D point in the model. In this case, the 3D model centroid is then the average position of the 3D vertices of the model. This point changes when the fragment position is displaced.

$$C_{x,y,z} = \frac{x_{x,y,z_1} + x_{x,y,z_2} + x_{x,y,z_3} + ...x_{x,y,z_k}}{k} \tag{4.1}$$

In the equation, are the finite number of points that represent a particular fragment. x_{x_k,y_k,z_k} are $'x'$,$'y'$and $'z'$ co-ordinates of k^{th}point of a fragment. The change in centroid of a displaced fragment gives an measure of its displacement. Higher translational displacement suggests higher fracture severity.

$$C_{\text{change}} = \sqrt{(x_{\text{m}} - x_{\text{a}})(x_{\text{m}} - x_{\text{a}}) + (y_{\text{m}} - y_{\text{a}})(y_{\text{m}} - y_{\text{a}}) + (z_{\text{m}} - z_{\text{a}})(z_{\text{m}} - z_{\text{a}})} \quad (4.2)$$

In the equation, C_{change} is the change in fracture fragment centroid C_f (x_f, y_f, z_f) and intact fragment centroid C_i (x_i, y_i, z_i).

The change in centroid position (translational displacement) is computed for every fragment for all the seven fracture cases. The translational displacement feature is taken as the sum of the centriod displacements for all the fracture fragments in a fracture case.

4.2.1.2 Angle Of Orientation

In addition to translation, high energy fractures often cause the bone fragment orientations to change. This "tumbling" action of the fragments is captured by measuring the angular change (rotational displacement) in the x, y, z axis of a fracture fragment between its aligned and misaligned position. The angular displacement is measured using the three Euler angles: α, β and γ which provide angular rotation actions on the fragment with respect to the z, y, x and axes respectively as depicted in Figure 4.2b. The values of these angle are set such that, when these rotations act on each fragment, they will change the fragment orientation from its fractured orientation to its proper anatomic orientation. These values give an estimate of the angular displacement of that particular fragment and indicate the amount of angular displacement. Once the change in the angle of orientation is obtained for every fragment, it is added across all the fragments to obtain a single score of angular displacement for that case. Assessment of the amount of displacement that the fracture fragments undergo affects the fracture treatment and pre-operative planning.

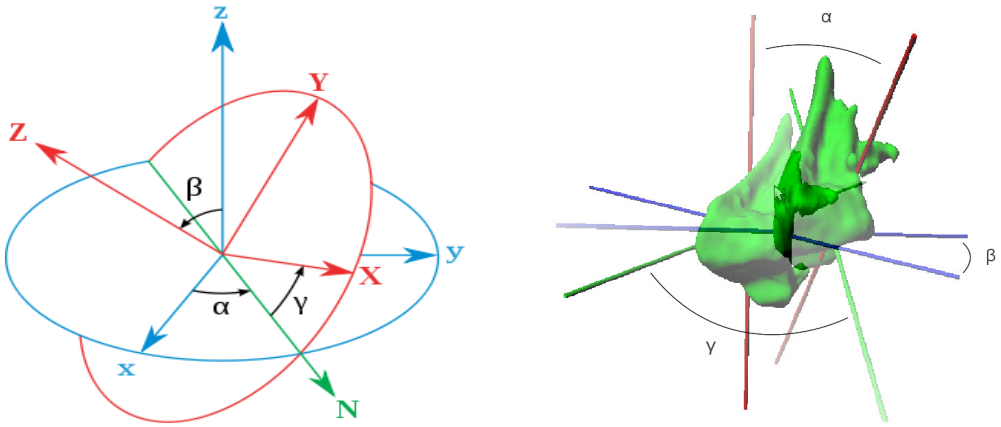

(a) (b)

Figure 4.2: Visual depiction of the angular displacement values (α, β, γ) as represented by the 3D Euler rotation.

Faint lines(blue, red and green): Fixed frame (aligned fragment).

Solid lines(blue, red and green): Frame under rotation (displaced fragment).

α: Angle between the z-axis (in red) of aligned fragment and displaced fragment.

β : Angle between the y-axis (in blue) of aligned fragment and displaced fragment.

γ : Angle between the x-axis (in green) of aligned fragment and displaced fragment.

The amount angular shift just describes the shift in axes and not the actual sequence of relocation Figure [4.2b]. This thesis considers change in angular orientation as one of the fracture measures to predict fracture severity.

These two displacement values are computed for every fragment of the seven fracture cases. Their respective summation act as two different fracture measures used to predict severity of a fracture. Higher displacement value suggests higher fracture severity.

4.2.2 Tissue Related Feature (Skewness Of Fracture Intensity Histogram)

Every fracture surface consists of 3D points, which are described by x, y, z coordinates. Fracture surface intensity profile of a fragment can be explained as a record of the intensity values at the points that lie on the fracture surface of that fragment. The intensity value captured at fragment points in its virtually reconstructed fracture

location inscribed in the intact template suggests whether they lie in cancellous or cortical tissue regions of the bone. High intensity values indicate that the points lie in locations of dense bone tissue (cortical) and smaller values indicate that they lie in locations of low-density bone tissue (cancellous). If a majority of the observed points are found to lie in high intensity regions, then the fragment was generated by fracturing, i.e., separating, rigid and strong cortical tissue area. If the majority of the observed points are found to lie in low intensity regions then the fragment was generated by fracturing weaker cancellous tissues. This behavior can be captured quantitatively by the statistical skewness of the histogram intensities observed as shown in Figure 4.4a

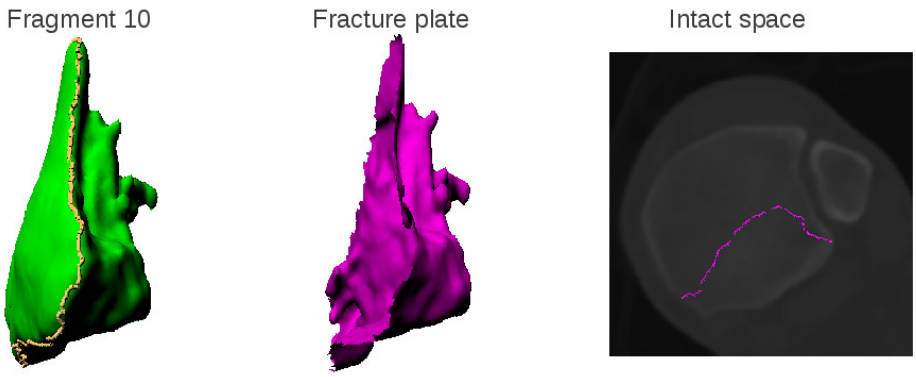

Figure 4.3: Fracture plate (surface) of a fragment inscribed in intact DICOM space. The fragment appears in green, the fracture plate appears in pink and its orientation is inscribed in intact space (DICOM) space in pink.

A bone fragment is segmented into numerous surfaces by applying ridge walking algorithm [43]. Every surface depicts a part of the surface of the bone, generated after the bone is fractured. Few surfaces are selected based on their anatomic significance, by observing and comparing the surface with the reference template, and are merged to form a single surface patch. The fracture surface is taken as the union of the articular and fracture patches. Those surface patches remaining are merged into a single periosteal (outer) surface patch which approximated the outer/intact surface of the fragment prior to the fracture event.

For every fragment, a group of fracture surfaces is rendered in the intact space to give their precise orientation. The intensity values of the CT image that lie along the fracture surface are obtained as shown in Figure 4.4b. These intensities are compiled into a fracture surface intensity histogram for every fragment in a given fracture case. Skewness of these histograms indicates the types of tissues sundered by the fracture event and is explored as a fracture feature for predicting fracture severity(Figure 4.5). This intensity profile (or histogram) of a fragment surface gives anatomic information of the fracture which can be used to evaluate the extent of fracture.

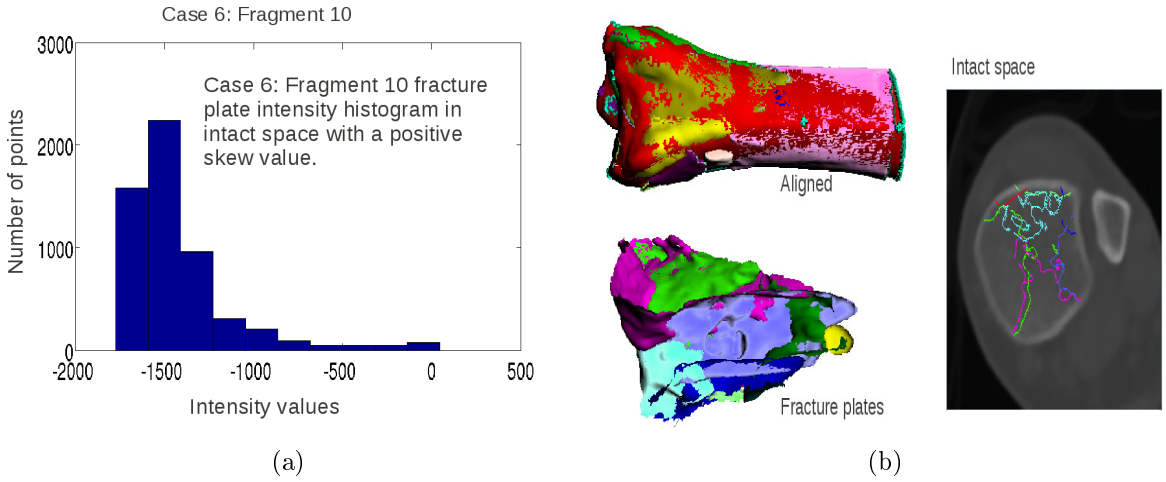

(a) (b)

Figure 4.4: (a) shows the fracture plate (surface) histogram. (b) shows the fracture plate surfaces of all fragments inscribed in intact space. The fragment and its respective orientation is displayed in intact space in same colors.

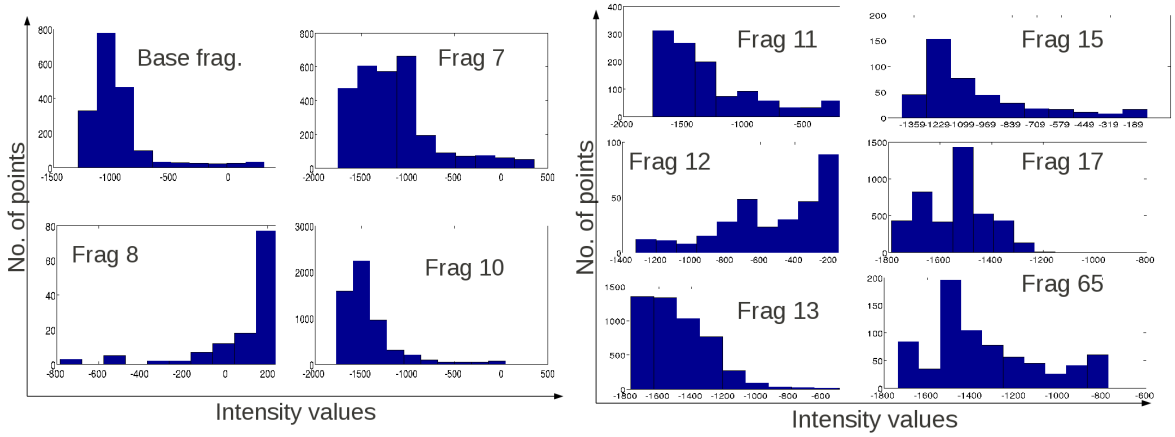

(a) (b)

Figure 4.5: Case 6: Fracture surface intensity histograms

Plots for every fragment in each case are generated, and required statistical data is gathered in chapter 5. This statistical data gives an idea as to where the fracture disruption is maximum, i.e., cancellous or cortical, which may be an effective predictor for fracture severity.

4.2.3 Mechanical Features (Fracture Surface Area And Fracture Surface Perimeter)

Fracture surfaces are generated when bone tissue breaks apart. Segmentation of the images of the bone fragments provides an estimate of the unknown bone fragment surfaces. The 3D model of a bone fragment is a mesh structure of triangles. The fracture surface obtained by performing ridge walking algorithm segmentation on this 3D model also results in a mesh, which is a subset of the parent bone fragment. The fracture surface area for the fracture surface is obtained by summing up the area of individual triangles. Given three vertices of a triangle V_0, V_1 and V_2 it's area is obtained by the cross product of it's edge vectors.

Accurate segmentations of the fracture surfaces is a crucial factor in the effective use of fracture surface area and fracture surface perimeter as features for predicting fracture severity. Overall, the accuracy of representation of a fracture surface depends

on the selection of a fracture region done by applying ridge walking algorithmic or by manually selecting a region. The accuracy can be increased by increasing the points i.e., by representing the 3D model of fracture surface by a denser set of points. Some patches are relatively smaller due to running segmentation algorithm multiple times. This is a tedious process and may lead to over segmentation. To avoid this, a contiguous surface patch can be obtained by manually selecting the region.

The perimeter of the entire fracture surface is an independent indicator to the fracture severity. It is defined as the summation of the lengths of the peripheral edges of a fracture surface, represented by pink border in Figure 4.6.

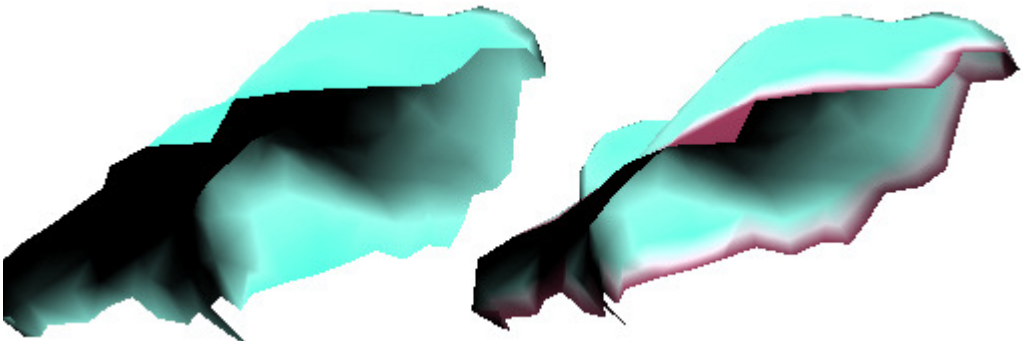

Figure 4.6: Fracture surface perimeter marked in pink

4.3 Linear Regression Analysis

In this section the performance of the computed fracture features is measured by exploring the correlation between these features and fracture severity values assigned by orthopaedic surgeons using linear regression. In this regard, we consider the goodness-of-fit as a measure of the feature performance and fit a line to (x, y) data where x values are taken as computed values of some fracture feature and y values are taken as fracture severity values assigned by the surgeons. The errors between the estimated line of best fit $y = mx + b$ and the measured data is taken as an indicator of how well the fracture feature predicts to fracture severity.

4.4 Correlation: Accuracy Of Reconstruction Measure

Correlation coefficient is a statistical tool to establish a degree of linear relation between two sets of observation. This reflects the similarity of nature between the sets of values. The correlation can range from -1 to 1. Positive correlation states a directly proportional relationship and negative correlation states an inverse relation. This is a dimensionless quantity and thus does not depend on units. The mathematical formula for correlation coefficient is given by

$$r = \frac{n\sum xy - (\sum x)(\sum y)}{\sqrt{n(\sum x^2) - (\sum x)^2}\sqrt{n(\sum y^2) - (\sum y)^2}} \tag{4.3}$$

In this equation, x are the fragment intensity values of the points constituting a fragment at a specific location in the DICOM space, y are the intensity values of the same fragment at a different location in the DICOM space and n is the number of points present in the fragment. The value of correlation coefficient(r) varies between $-1 < 0 < 1$. Ranges for these values indicate specific relative trends for the values of x and y as follows:

- **Positive correlation:** A strong positive 'r' suggests a linear relation i.e, as the fracture intensity values for a particular fragment remains similar for x and y.
- **Negative correlation:** A strong negative 'r' suggests an inverse relation i.e, as the fracture intensity values for a particular fragment changes drastically for x and y.

In this thesis correlation is used to evaluate the accuracy of virtually reconstructed bone. The accuracy of an aligned fracture fragment is evaluated by computing two correlation values. Given the tissues of the intact template bone model, the tissues of the bone fragment are correlated to those tissues in the same space, i.e., coincident location, in the template model. Before reconstruction Figure 4.4a, the bone fragment tissue will differ from the tissues at coincident locations in the intact template bone

model resulting in a low or possibly negative correlation. After reconstruction Figure 4.4a, the bone fragment tissue will be similar to the tissues at coincident locations in the intact template bone model resulting in a highly positive correlation value. If this trend is not observed one can hypothesize that the bone fragment alignment in the intact template bone model may not be accurate.

The correlation value for the base fragment remains same for both the cases as the position of the base fragment does not change in the intact space or fracture space. Computing correlation can be made more robust by increasing the number of sample points that represents a fragment volume.

CHAPTER 5: CLINICAL CASE-WISE RESULTS AND ANALYSIS

This chapter discusses seven clinical fracture cases. For each case, the proposed five fracture features: (1) total fracture translational displacement, (2) total fracture angular displacement, (3) skewness of fracture surface intensity profile, (4) total fracture surface area and (5) total fracture surface perimeter are extracted. Typically these features are extracted from each bone fragment of the case separately and their values are subsequently merged by summing or averaging the feature values across the bone fragments of the case. The cases and their respective fracture feature values are tabulated and an initial discussion and case-specific analysis is provided. The numbering of each fracture case and of the fragments within the case is kept consistent with those assigned in a global fracture study database. This restriction on numbering results in a non-sequential numbering of the cases.

5.1 Case 6: MVA 50mph

5.1.1 Feature 1 And 2: Total Translational And Angular Displacement Measure

Every fragment undergoes translational and angular displacement depending on the direction and magnitude of the force responsible for generating the fracture. Figure 5.1(c) shows the fragment translational displacement in intact space and Figure 5.1(a) shows how far it lies from the reference template in the intact space. As observed from the following table, frag10 undergoes high translational as well as angular displacement while frag8 undergoes minimum angular and translational displacement. The translational and angular displacement (α, β, γ) of all the fragments is added respectively to get fracture measure values.

Table 5.1: Case 6: Fracture fragment-based translational and angular displacement values with the translational and angular fracture feature values indicated in bold.

Frag no.	Translational measure (mm)	α (°)	β (°)	γ(°)	Total angular displacement (°)
frag10	13.01	27.6	48.24	45.52	121.3
frag11	14.9	30.43	21.3	21.7	73.43
frag12	4.32	12.64	24.48	25.02	62.14
frag13	7.7	25.06	42.05	48.78	115.29
frag15	0.31	6.43	9.66	7.97	24.06
frag17	14.05	41.48	19.59	45.36	106.43
frag5	0	0	0	0	0
frag65	12.40	59.65	62.39	29.51	151.55
frag7	15.39	34.72	17.24	31.46	83.42
frag8	1.01	11.08	7.12	9.32	27.52
Total	**83.09**	885.66	252.07	264.64	**765.74**

5.1.2 Feature 3: Skewness Of Fracture Surface Intensity Profile

The statistical data obtained from all the fragments in this case is tabulated in Table 5.2. The skewness value evaluates the intensity distribution of the CT intensities that occur at fracture surface points and provides a coarse indication of whether the fracture surface passes through mostly cancellous tissues or mostly cortical tissues. A positive skew value indicates higher presence of cancellous bone tissue on the fracture surface and a negative skew value indicates a high presence of cortical bone tissue (Table 5.2). The average skewness value for this case suggests a dominant cancellous bone presence along the fracture surface. Since, the fracture surface points dominantly lie in the cancellous bone (less dense) region, the severity of the fracture is suggested

to be not very high.

Table 5.2: Case 6: Key parameters of the fracture surface intensity distribution including skewness and other statistical data for fracture surface intensity profile. The skewness fracture feature value is shown in bold.

Frag #	mean	median	mode	skewness	std
Frag 10	-1419.9	-1484	-1496	2.32	303.00
Frag 11	-1247.1	-1401	-1736	1.09	460.16
Frag 12	-527.54	-460.50	-347	-0.70	308.73
Frag 13	-1477.1	-1500	-1498	1.29	211.02
Frag 15	-1042.6	-1147.5	-1281	1.40	299.59
Frag 17	-1537.1	-1510	-1504	0.12	125.14
Frag 5	-939.93	-1004	-1024	2.39	284.58
Frag 65	-1335.5	-1422	-1495	0.61	256.07
Frag 7	-1157.4	-1264	-1024	1.15	444.25
Frag 8	81.4206	166	191	-2.29	222.62
Average				**0.738**	

5.1.3 Feature 4 and 5: Total Fracture Surface Area (FSA) And Total Fracture Surface Perimeter (FSP)

Higher surface area indicates high disruption in the intact anatomy and thus a higher severity. Table 5.3 tabulates the FSA and FSP values for all the fragments involved in this case. Their total FSA and FSP are considered as fracture measures to evaluate severity. These measures are shown in Table 5.29. Articular area and articular perimeter is also computed in an effort to analyze the extent of fracture severity. Higher articular damage suggests high fracture severity as articular damage is known to cause significant damage to joint structure and functionality. However, they are not considered as separate fracture features as the are a part of FSA and

FSP fracture features.

Table 5.3: Case 6: Fracture surface area and surface perimeter features are computed for each fracture fragment. These values are summed to generate the case FSA and FSP fracture feature values which are shown in bold.

Frag #	FSA	Articular Area	Total FSA	FSP	Articular perimeter
Frag 10	1562.09	666.26	2228.35	8031.73	3574.13
Frag 11	456.31	-	456.31	2360.34	-
Frag 12	124.57	-	124.57	614.61	
Frag 13	2081.15	273.91	2355.06	10160.67	1462.11
Frag 15	161.42	-	161.42	841.93	-
Frag 17	1227.78	234.75	1462.53	8581.57	1277.09
Frag 5	698.32	-	698.32	3795.59	-
Frag 6	292.07	-	292.07	1445.42	-
Frag 7	1129.64	-	1129.64	5802.65	-
Frag 8	53.84	-	53.84	241.99	-
Total (10)	**7787.19**	1174.92	**8962.11**	41876.5	6313.33

5.1.4 Correlation: Accuracy Of Reconstruction Measure

After reconstruction, the aligned fragments must have a high agreement with respect to their position in intact template. As expected, Table 5.4 shows an increase in correlation, for all the fragments, after virtual reconstruction. Higher values of the correlation coefficients generally indicate a better quality in the geometric reconstruction.

Table 5.4: Case 6: Correlation between the gray scale intensities at the fragment positions in the intact and fracture DICOM, before and after the alignment.

Case 6		Correlation	
Frag #	No. of surface points	Before align5.1(b),(c)	After align5.1(c),(d)
Frag 10	8987	0.47	0.57
Frag 11	2373	0.12	0.72
Frag 12	594	0.12	0.64
Frag 13	9595	0.47	0.52
Frag 15	732	0.12	0.21
Frag 17	6168	0.31	0.39
Frag 5	16359	0.54	0.54
Frag 65	1515	0.13	0.24
Frag 7	5312	0.72	0.68
Frag 8	223	0.44	0.46

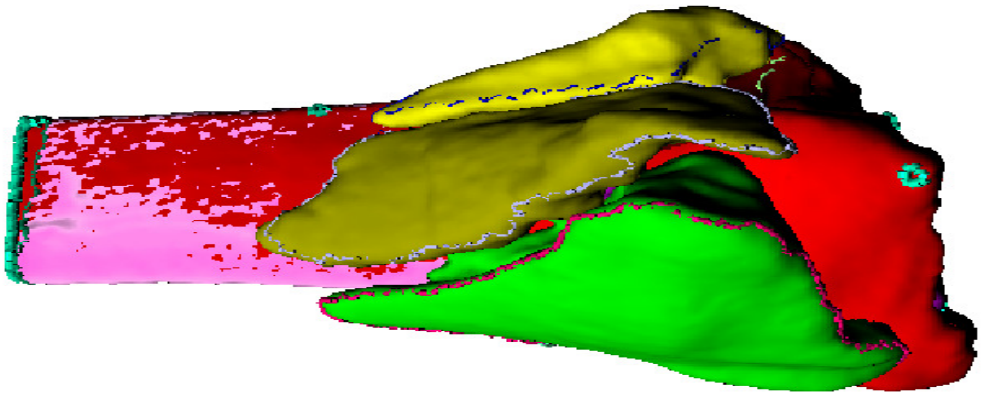

(a)

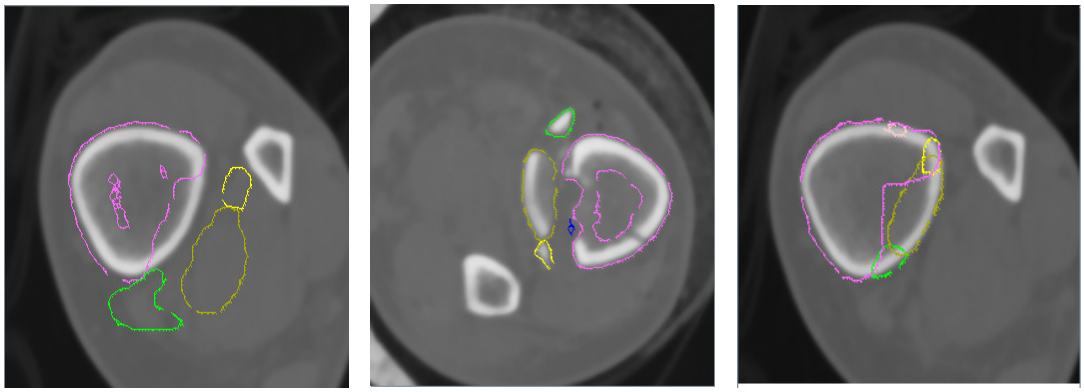

(b) (c) (d)

Figure 5.1: Case 6: Correlation computation and evaluation. (a) shows a 3D visualization of the fracture case before reconstruction. (b) shows fragment contours superimposed on an axial CT image of the intact bone template. The contours appear far away from the intact bone suggesting significant fragment displacement 5.1.1. (c) shows fragment contours superimposed on an axial CT image of the fracture. The contours of bone fragments coincide with the fragment surfaces in the CT suggesting that the segmentation of these fragments is acceptable.(d) shows fragment contours superimposed on an axial CT of the intact bone template. Here, the fragments have been moved to reconstruct a model of the bone prior to the injury.

'Before Align' suggests correlation between Figure 5.1(b) and Figure 5.1(c). 'After align' lists correlation between Figure 5.1(c) and Figure 5.1(d).

5.1.5 Analysis

As shown, even though the correlation numbers display a good virtual reconstruction of the fractured bone, the number of fragments and high displacement of a

fragment with a large surface area indicate that this was a severe fracture involving a large force. The extent of surface disruption of the articular joint surfaces indicate that this case fracture will be predisposed to developing OA. Overall, fragment displacement and large articular tissue rupture indicate severe fracture. It can be inferred that this given case suffered severe fracture.

5.2 Case 7: A 30 Foot Fall

5.2.1 Feature 1 and 2: Total Translational And Angular Displacement Measure

Figure 5.2(c) and Figure 5.2(a), depictvisually the degree of dispersion/translation of the bone fragments. The large amount of dispersion observed visually is confirmed by the feature values shown in Table 5.5. Here one can see that fragment 4 (frag 4) undergoes high translational as well as angular displacement while fragment 2 (frag 2) undergoes a small amount of angular and translational displacement.

Table 5.5: Case 7: Fracture fragment-based translational and angular displacement values with the translational and angular fracture feature values indicated in bold.

Frag no.	Translational measure (mm)	α (°)	β (°)	γ (°)	Total angular displacement (°)
Frag 1	0	0	0	0	0
Frag 2	8.82	16.46	16.44	19.02	51.92
Frag 3	8.04	26.98	26.21	28.88	82.07
Frag 4	18.17	127.45	71.75	141.04	340.24
Frag 5	15.14	102.76	73.42	130.23	306.41
Frag 6	12.95	63.83	57.13	62.14	183.1
	63.12	337.48	244.95	381.31	**963.74**

5.2.2 Feature 3: Skewness Of Fracture Surface Intensity Profile

The statistical data obtained from all the fragments in this case is tabulated in Table 5.6. The skewness value evaluates the distribution of the fracture surface points between cancellous region and cortical region. The average skewness value for this case suggests a dominant cancellous bone presence along the fracture surface. Note that frag4, frag5, frag6 are not visible in Figure 5.1 due to the fact that they are small fragments that are internal to the bone, hence not visible from an exterior view.

Table 5.6: Case 7: Key parameters of the fracture surface intensity distribution including skewness and other statistical data for fracture surface intensity profile. The skewness fracture feature value is shown in bold.

Frag #	mean	median	mode	skewness	std	var
Frag 1	-1.1344e+03	-1101	-1024	1.2868	278.4192	7.7517e+04
Frag 2	-1.1389e+03	-1151	-1024	1.6197	333.5329	1.1124e+05
Frag 3	-1.1541e+03	-1141	-1024	0.6895	250.2770	6.2639e+04
Frag 4	-1.5057e+03	-1542	-1582	0.5584	119.4907	1.4278e+04
Frag 5	-1.5890e+03	-1595	-1627	0.5545	45.8385	2.1012e+03
Frag 6	-1.5616e+03	-1581	-1729	0.5500	144.1817	2.0788e+04
Average				**0.87**		

5.2.3 Feature 4 and 5: Total Fracture Surface Area (FSA) And Total Fracture Surface Perimeter (FSP)

Table 5.7 tabulates FSA and FSP values for all the fragments involved in this case.

Table 5.7: Case 7: Fracture surface area and surface perimeter features are computed for each fracture fragment. These values are summed to generate the case FSA and FSP fracture feature values which are shown in bold.

Frag no.	FSA	Articular Area	Total FSA	FSP	Articular perimeter
Frag 1	2336.15	331.25	2667.4	25742.41	894.65
Frag 2	1941.06	100.59	2041.65	17991.76	984.73
Frag 3	959.45	93.28	1052.73	8187.37	950.24
Frag 4	651.13	103.03	754.16	4301.01	877.92
Frag 5	265.18	73.58	338.76	1611.64	751.69
Frag 6	94.09	-	94.09	408.79	-
	6247.06	701.73	**6948.79**	**58242.98**	4459.23

5.2.4 Correlation: Accuracy Of Reconstruction Measure

For case 7, in Table 5.8 as expected, there is an increase in correlation after alignment, for all the fragments. Better alignment indicates better reconstruction.

Table 5.8: Case 7: Correlation between the gray scale intensities at the fragment positions in the intact and fracture DICOM, before and after the alignment.

Case 7		Correlation	
Frag #	No. of surface points	Before align 5.2 (b), (c)	After align 5.2 (c), (d)
Frag 1	87844	0.59	0.59
Frag 2	34119	0.76	0.63
Frag 3	17970	0.73	0.84
Frag 4	4299	0.21	0.66
Frag 5	2716	0.03	0.83
Frag 6	325	0.66	0.80

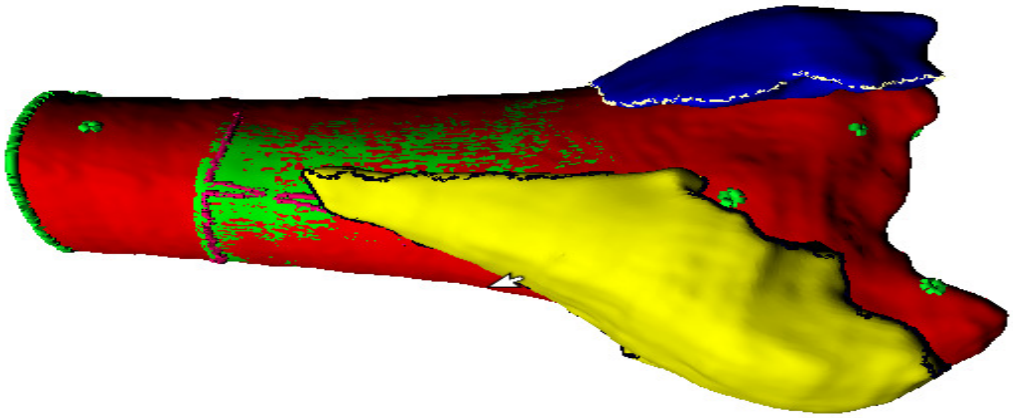

(a)

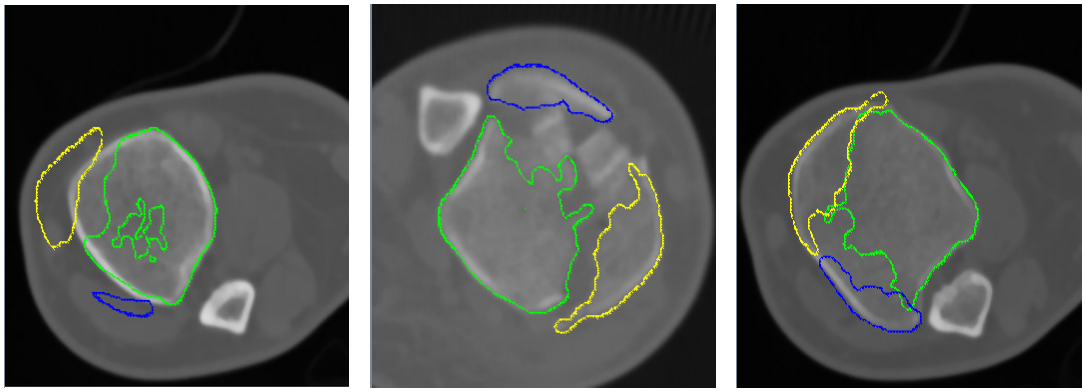

(b) (c) (d)

Figure 5.2: Case 7: Correlation computation and evaluation (a) shows a 3d visualization of the misaligned fragments of case 7. (b) shows misaligned fragments' contour inscribed in its intact template in DICOM. The fracture contours appear away from the intact bone suggesting significant fracture displacement. (c) shows misaligned fragments' contour inscribed in its fracture DICOM image. The contours of fracture fragments coincide with the fracture contours in DICOM suggesting acceptable amount of accuracy in the inscription process. (d) shows fracture fragments' location of 3d reconstructed model inscribed in an intact DICOM template.

'Before Align' suggests correlation between Figure 5.2(b) and Figure 5.2(c). 'After align' lists correlation between Figure 5.2(c) and Figure 5.2(d).

5.2.5 Analysis

The correlation numbers display a good virtual reconstruction of the fractured bone. With a medium number of fragments, the average translational displacement

and large angular displacement this case suggests trauma that is less severe than case 6. Large angular displacements disturb local tissue structures dominantly in cancellous region indicating long healing process. Overall, medium number of fragments, fragment displacement and local tissue damage indicate medium severity fracture.

5.3 Case 8: MVA 30mph

5.3.1 Feature 1 and 2: Total Translational And Angular Displacement Measure

Figure 5.3(b) and Figure 5.3(d), gives a graphical reference to view the fragment translational displacement in intact space. As observed from the following table, frag 5 undergoes high translational as well as angular displacement while frag 7 undergoes minimum angular and translational displacement.

Table 5.9: Case 8: Fracture fragment-based translational and angular displacement values with the translational and angular fracture feature values indicated in bold.

Frag no.	Translational measure	$\alpha(^{o})$	$\beta(^{o})$	$\gamma(^{o})$	Total angular displacement $(^{o})$
Frag 1	0	0	0	0	0
Frag 2	11.94	89.59	68.48	101.5	259.57
Frag 4	14.96	54.47	42.28	54.63	151.38
Frag 5	26.77	16.07	9.34	18.59	44
Frag 7	4.62	39.45	21.15	43.02	103.62
Frag 8	12.16	40.50	76.34	76.82	193.66
	70.45	240.08	217.59	294.56	**752.23**

5.3.2 Feature 3: Skewness Of Fracture Surface Intensity Profile

The statistical data obtained from all the fragments in this case is tabulated in Table 5.10. The average skewness value for this case suggests a dominant cancellous bone presence along the fracture surface.

Table 5.10: Case 8: Key parameters of the fracture surface intensity distribution including skewness and other statistical data for fracture surface intensity profile. The skewness fracture feature value is shown in bold.

Frag #	mean	median	mode	skewness	std	var
1	-982.5588	-1060	-1024	2.2816	311.2765	9.6893e+04
2	-421.1793	-579.5000	-1111	0.2384	673.8425	4.5406e+05
4	-396.0615	-302	-91	-0.0847	551.6681	3.0434e+05
5	-1.2201e+03	-1239	-1137	1.4273	357.2718	1.2764e+05
7	-1.1248e+03	-1169	-1197	1.7585	156.8803	2.4611e+04
8	-1.5003e+03	-1548	-1628	0.3733	175.9812	3.0969e+04
Average				**0.99**		

5.3.3 Feature 4 and 5: Total Fracture Surface Area (FSA) And Total Fracture Surface Perimeter (FSP)

Table 5.11 tabulates FSA and FSP values for all the fragments involved in this case. Minimal presence of articular region can also be inferred from the table below.

Table 5.11: Case 8: Fracture surface area and surface perimeter features are computed for each fracture fragment. These values are summed to generate the case FSA and FSP fracture feature values which are shown in bold.

Frag no.	FSA	Articular Area	Total FSA	FSP	Articular perimeter
Frag1	3192.78	-	3192.78	20673.64	-
Frag2	380.76	-	380.76	2362.82	-
Frag4	237.98	-	237.98	1462.23	-
Frag 5	2454.19	481.26	2935.45	16005.76	3017.42
Frag 7	132.76	-	132.76	856.91	-
Frag 8	1474.03	473.99	1948.02	9471.46	3295.80
	7872.5	955.25	**8827.75**	**50832.82**	6313.22

5.3.4 Correlation: Accuracy Of Reconstruction Measure

From Table 5.12 for case 8, an increase is seen in correlation after alignment for all the fragments. Better alignment indicates better reconstruction.

Table 5.12: Case 8: Correlation between the gray scale intensities at the fragment positions in the intact and fracture DICOM, before and after the alignment.

Case 8		Correlation	
Frag #	No. of surface points	Before align 5.3 (b), (c)	After align 5.3 (b), (c)
Frag 1	29007	0.27	0.27
Frag 2	3105	0.05	0.47
Frag 4	1600	0.01	0.49
Frag 5	23779	0.10	0.18
Frag 7	945	0.14	0.06
Frag 8	11652	0.06	0.29

'Before Align' suggests correlation between Figure 5.3(b) and Figure 5.3(c). 'After align' lists correlation between Figure 5.3(c) and Figure 5.3(d). With decrease in total number of points in the fragment, the correlation value gets affected. Thus, Frag 7 shows a decrease in its correlation value.

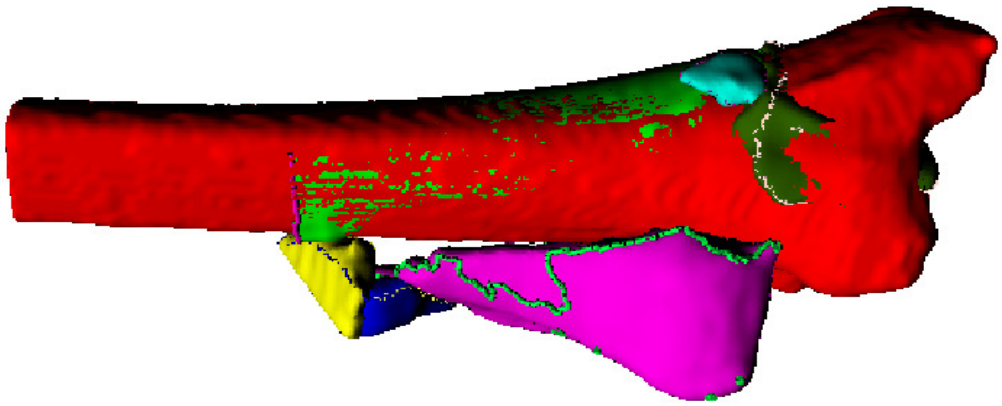

(a)

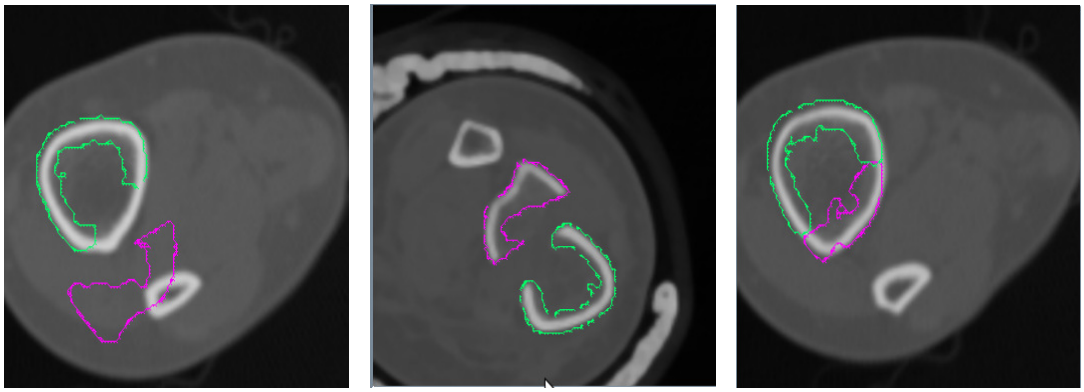

(b) (c) (d)

Figure 5.3: Case 8: Correlation computation and evaluation (a) shows a 3d visualization of the misaligned fragments of case 8. (b) shows misaligned fragments' contour inscribed in its intact template in DICOM. The fracture contours appear away from the intact bone suggesting significant fracture displacement. (c) shows misaligned fragments' contour inscribed in its fracture DICOM image. The contours of fracture fragments coincide with the fracture contours in DICOM suggesting acceptable amount of accuracy in the inscription process. (d) shows fracture fragments' location of 3d reconstructed model inscribed in an intact DICOM template.

5.3.5 Analysis

The correlation numbers display a average quality of virtual reconstruction of the fractured bone since maximum correlation value increase is ~0.5. With medium number of fragments, average translational displacement and large angular displacement this case suggests a low force trauma. Large angular displacement disturbs the local tissue structure, dominantly in cancellous region indicating long healing process. Overall, medium number of fragments, fragment displacement, local tissue damage indicate medium severity fracture.

5.4 Case 9: All-Terrain Vehicle Accident

5.4.1 Feature 1 and 2: Total Translational And Angular Displacement Measure

Figure 5.4(b) and Figure 5.4(d) gives a graphical reference to view the fragment translational displacement in intact space. As observed from the following table, frag 2 undergoes high translational whereas low angular displacement while frag3 undergoes large angular and low translational displacement.

Table 5.13: Case 9: Fracture fragment-based translational and angular displacement values with the translational and angular fracture feature values indicated in bold.

Frag no.	Translational measure (mm)	$\alpha(^o)$	$\beta(^o)$	$\gamma(^o)$	Total angular displacement (^{o})
Frag 1	0	0	0	0	0
Frag 2	4.2	8.03	7.08	5.38	20.49
Frag 3	3.52	20.06	8.22	20.72	49
	7.72	28.09	15.3	26.1	**69.49**

5.4.2 Feature 3: Skewness Of Fracture Surface Intensity Profile

The statistical data obtained from all the fragments in this case is tabulated in Table 5.14. The skewness value suggests a dominant cancellous bone presence along the fracture surface.

Table 5.14: Case 9: Key parameters of the fracture surface intensity distribution including skewness and other statistical data for fracture surface intensity profile. The skewness fracture feature value is shown in bold.

Frag #	mean	median	mode	skewness	std	var
Frag 1	-1.1951e+03	-1260	-1323	1.1054	394.6038	1.5571e+05
Frag 2	-1.3847e+03	-1442	-1690	1.3853	311.8241	9.7234e+04
Frag 3	-1.5650e+03	-1588	-1606	0.4521	150.9959	2.2800e+04
				0.97		

5.4.3 Feature 4 and 5: Total Fracture Surface Area (FSA) And Total Fracture Surface Perimeter (FSP)

Table 5.15 tabulates FSA and FSP values for all the fragments involved in this case.

Table 5.15: Case 9: Fracture surface area and surface perimeter features are computed for each fracture fragment. These values are summed to generate the case FSA and FSP fracture feature values which are shown in bold.

Frag no.	FSA	Articular Area	Total FSA	FSP	Articular perimeter
Frag 1	7712.39	86.30	7798.69	19542.56	601.34
Frag 2	3101.19	567.45	3668.64	13440.06	3850.30
Frag 3	1805.71	194.55	2000.26	8015.28	1175.52
	12619.29	848.31	**13467.59**	**40997.9**	5627.17

5.4.4 Correlation: Accuracy Of Reconstruction Measure

Similar to Case 6, an observation is drawn from Table 5.16 for case 9. As expected, an increase is seen in correlation, for all the fragments, from scenario 1 to scenario 2. Better alignment indicates better reconstruction.

Table 5.16: Case 9: Correlation between the gray scale intensities at the fragment positions in the intact and fracture DICOM, before and after the alignment.

Case 9		Correlation	
Frag #	No.of surface points	Before align5.4 (b), (c)	After align5.4 (c), (d)
Frag 1	36046	0.54	0.54
Frag 2	15194	0.79	0.86
Frag 3	8324	0.68	0.89

'Before Align' suggests correlation between Figure 5.4(b) and Figure 5.4(c). 'After align' lists correlation between Figure 5.4(c) and Figure 5.4(d).

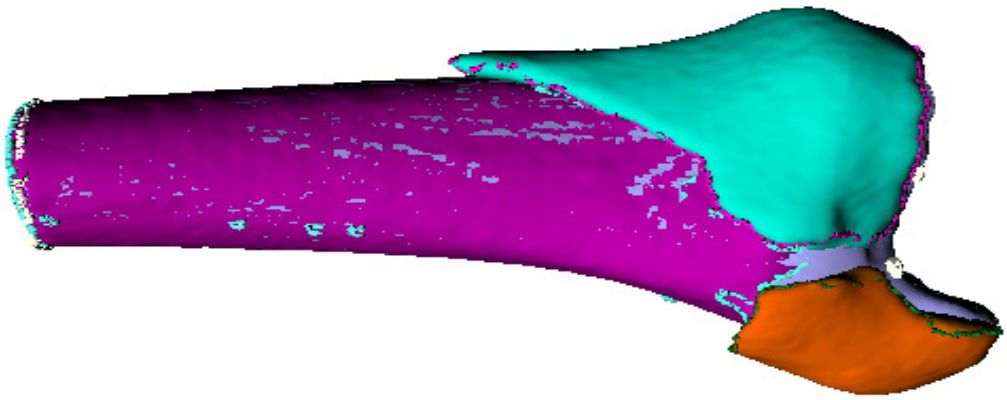

(a)

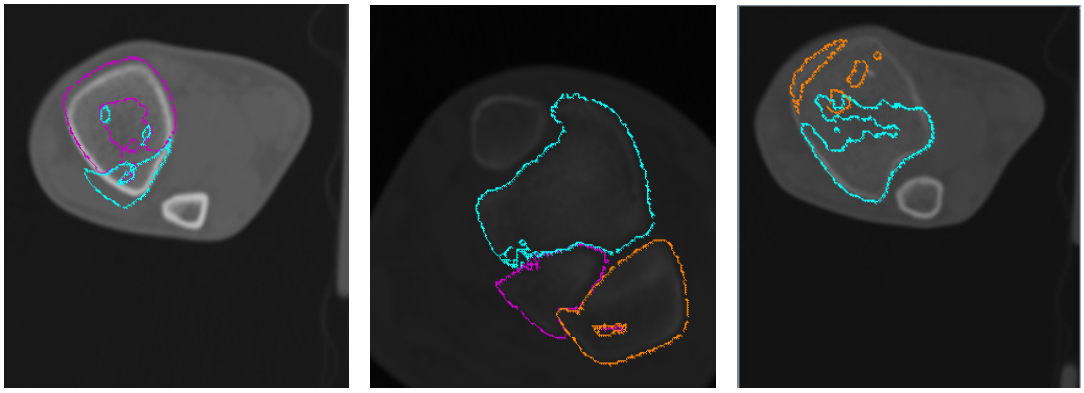

(b) (c) (d)

Figure 5.4: Case 9: Correlation computation and evaluation (a) shows a 3d visualization of the misaligned fragments of case 9. (b) shows misaligned fragments' contour inscribed in its intact template in DICOM. The fracture contours appear away from the intact bone suggesting significant fracture displacement. (c) shows misaligned fragments' contour inscribed in its fracture DICOM image. The contours of fracture fragments coincide with the fracture contours in DICOM suggesting acceptable amount of accuracy in the inscription process. (d) shows fracture fragments' location of 3d reconstructed model inscribed in an intact DICOM template.

5.4.5 Analysis

The correlation numbers display a very good quality of virtual reconstruction of the fractured bone since maximum correlation value increase is ~0.88. With three large size fragments and small translational and angular displacement this case suggests a low force trauma. Overall, with almost 90% accurate reconstruction and very minimal articular damage this fracture case can be inferred to be not very severe.

5.5 Case 10: Fall 12 feet

5.5.1 Feature 1 and 2: Total Translational And Angular Displacement Measure

Figure 5.5(b) and Figure 5.5(d) gives a graphical reference to view the fragment translational displacement in intact space. As observed from the following table, frag 5 undergoes high translational as well as angular displacement while frag 2 undergoes minimum angular and translational displacement.

Table 5.17: Case 10: Fracture fragment-based translational and angular displacement values with the translational and angular fracture feature values indicated in bold.

Frag no.	Translational measure (mm)	$\alpha(^o)$	$\beta(^o)$	$\gamma(^o)$	Total angular displacement (^{o})
Frag 1	0	0	0	0	0
Frag 2	2.89	4.04	8.59	8.26	20.89
Frag 3	1.51	4.82	8.08	8.16	21.06
Frag 5	5.61	27.36	34.91	33.88	96.15
	10.01	36.22	51.58	50.3	**138.1**

5.5.2 Feature 3: Skewness Of Fracture Surface Intensity Profile

The statistical data obtained from all the fragments in this case is tabulated in Table 5.18. The skewness value suggests a dominant cancellous bone presence along the fracture surface.

Table 5.18: Case 10: Key parameters of the fracture surface intensity distribution including skewness and other statistical data for fracture surface intensity profile. The skewness fracture feature value is shown in bold.

Frag #	mean	median	mode	skewness	std	var
Frag 1	-396.9180	-647	-1024	0.2556	599.4591	3.5935e+05
Frag 2	-649.6017	-844.5000	-1014	1.3683	476.1138	2.2668e+05
Frag 3	-493.0478	-772	-1024	0.6778	526.7173	2.7743e+05
Frag 4	-922.9415	-934	-1024	1.5384	312.4488	9.7624e+04
Average				**0.97**		

5.5.3 Feature 4 and 5: Total Fracture Surface Area (FSA) And Total Fracture Surface Perimeter (FSP)

Table 5.19 tabulates FSA and FSP values for all the fragments involved in this case.

Table 5.19: Case 10: Fracture surface area and surface perimeter features are computed for each fracture fragment. These values are summed to generate the case FSA and FSP fracture feature values which are shown in bold.

Frag no.	FSA	Articular Area	Total FSA	FSP	Articular perimeter
Frag 1	3717.74	-	3717.74	13138.49	-
Frag 2	7042.83	567.99	7610.82	31580.42	3120.53
Frag 3	2991.58	-	2991.58	15062.89	-
Frag 5	4210.26	340.52	4550.78	17961.77	1928.67
	17962.41	908.51	**18870.92**	**77743.58**	5049.20

5.5.4 Correlation: Accuracy Of Reconstruction Measure

From Table 5.20 for case 10, as expected, an increase is seen in correlation for all the fragments, after alignment. Better alignment indicates better reconstruction.

Table 5.20: Case 10: Correlation between the gray scale intensities at the fragment positions in the intact and fracture DICOM, before and after the alignment.

Case 10		Correlation	
Frag #	No. of surface points	Before align5.5 (b), (c)	After align5.5 (c), (d)
Frag 1	20299	0.59	0.59
Frag 2	36385	0.25	0.38
Frag 3	14388	0.35	0.61
Frag 4	18255	0.31	0.47

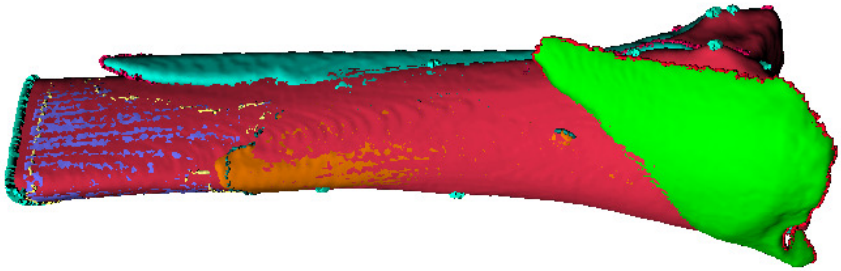

(a)

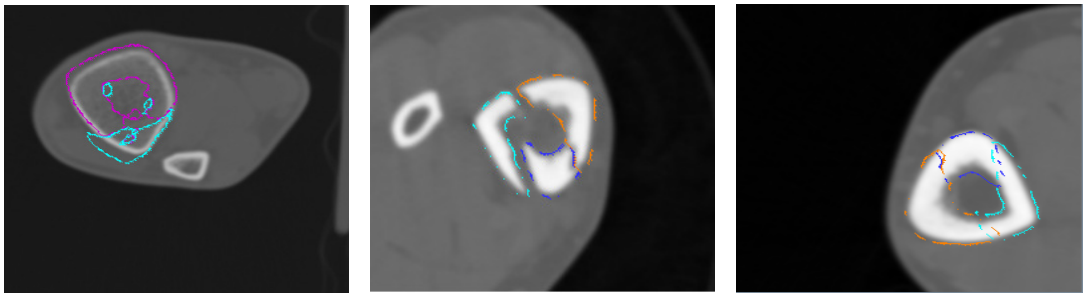

(b) (c) (d)

Figure 5.5: Case 10: Correlation computation and evaluation (a) shows a 3d visualization of the misaligned fragments in case 10. (b) shows misaligned fragments' contour inscribed in its intact template in DICOM. The fracture contours appear away from the intact bone suggesting significant fracture displacement. (c) shows misaligned fragments' contour inscribed in its fracture DICOM image. The contours of fracture fragments coincide with the fracture contours in DICOM suggesting acceptable amount of accuracy in the inscription process. (d) shows fracture fragments' location of 3d reconstructed model inscribed in an intact DICOM template.

'Before Align' in correlation between Figure 5.5(b) and Figure 5.5(c), i.e., intensities of misaligned fracture point position in intact and fracture DICOM. 'After align' lists correlation between Figure 5.5(c) and Figure 5.5(d).

5.5.5 Analysis

The correlation numbers display a very good quality of virtual reconstruction of the fractured bone since maximum correlation value increase is ~0.65. With large size fragments and small translational and angular displacement this case suggests a low force trauma. Overall, with almost 70% accurate reconstruction and very minimal articular damage this fracture case can be inferred as not very severe.

5.6 Case 11: Fall 18 Feet

5.6.1 Feature 1 and 2: Total Translational And Angular Displacement Measure

Figure 5.6(b) and Figure 5.6(d) gives a graphical reference to view the fragment translational displacement in intact space. As observed from the following table, frag2 undergoes minimum angular and translational displacement.

Table 5.21: Case 11: Fracture fragment-based translational and angular displacement values with the translational and angular fracture feature values indicated in bold.

Frag #	Translational measure (mm)	$\alpha(^o)$	$\beta(^o)$	$\gamma(^o)$	Total angular displacement (^{o})
Frag 1	0	0	0	0	0
Frag 10	10.31	24.16	17.02	27.54	68.72
Frag 2	2.39	2.21	6.22	6.59	15.02
Frag 4	7.56	26.55	29.88	26.05	82.48
Frag 5	6.53	20.17	20.27	16.41	56.85
Frag 6	8.57	30.15	16.66	29.29	76.1
Frag 8	7.52	13.87	11.92	7.38	33..17
Frag 9	8.05	37.28	15.00	39.93	92.21
	52.27	154.41	116.97	153.19	**362.55**

5.6.2 Feature 3: Skewness Of Fracture Surface Intensity Profile

The statistical data obtained from all the fragments in this case is tabulated in Table 5.22. The skewness value suggests a dominant cortical bone presence along the fracture surface.

Table 5.22: Case 11: Key parameters of the fracture surface intensity distribution including skewness and other statistical data for fracture surface intensity profile. The skewness fracture feature value is shown in bold.

Frag #	mean	median	mode	skewness	std	var
Frag 1	-12.309	-73	-81	1.78	200.77	4.0310e+04
Frag 10	-451.9138	-416	-743	0.1005	226.50	5.1304e+04
Frag 2	65.269	-25	-166	0.899	258.06	6.6598e+04
Frag 4	-259.94	-222	-166	-0.6804	208.5734	4.3503e+04
Frag 5	-363.4124	-308	-341	-0.2055	259.036	6.7100e+04
Frag 6	-438.4335	-356	-319	-0.7821	172.9495	2.9912e+04
Frag 8	-323.1215	-237	-166	-0.4500	307.9565	9.4837e+04
Frag 9	-525.5003	-478	-265	-1.1139	258.6549	6.6902e+04
Average				**-0.06**		

5.6.3 Feature 4 and 5: Total Fracture Surface Area (FSA) And Total Fracture Surface Perimeter (FSP)

Table 5.23 tabulates FSA and FSP values for all the fragments involved in this case.

Table 5.23: Case 11: Fracture surface area and surface perimeter features are computed for each fracture fragment. These valeus are summed to generate the case FSA and FSP fracture feature values which are shown in bold.

Frag #	FSA	Articular Area	Total FSA	FSP	Articular perimeter
Frag 1	5123.81	-	5123.81	31465.78	-
Frag 10	616.72	28.22	644.94	4138.16	244.13
Frag 2	3307.45	-	3307.45	21943.04	-
Frag 4	5535.61	115.38	5650.99	36287.29	1020.82
Frag 5	1079	-	1079	7800.56	-
Frag 6	1229.24	132.73	1361.97	6292.47	1139.71
Frag 8	3933.73	321.69	4255.42	23223.59	2822.30
Frag 9	2340.51	204.16	2544.67	18017.42	1713.146
	23166.07	802.18	**23968.25**	**149168.3**	6940.106

5.6.4 Correlation: Accuracy Of Reconstruction Measure

From Table 5.24 for case 11. As expected, an increase is seen in correlation, for all the fragments, after alignment. Better alignment indicates better reconstruction.

Table 5.24: Case 11: Correlation between the gray scale intensities at the fragment positions in the intact and fracture DICOM, before and after the alignment.

Case 11		Correlation	
Frag #	No. of surface points	Before align5.6 (b), (c)	After align5.7 (c), (d)
Frag 1	39160	0.73	0.73
Frag 10	4305	0.30	0.79
Frag 2	20307	0.71	0.76
Frag 4	33488	0.40	0.59
Frag 5	7045	0.42	0.70
Frag 6	5548	0.54	0.69
Frag 8	30423	0.44	0.66
Frag 9	16476	-0.28	0.11

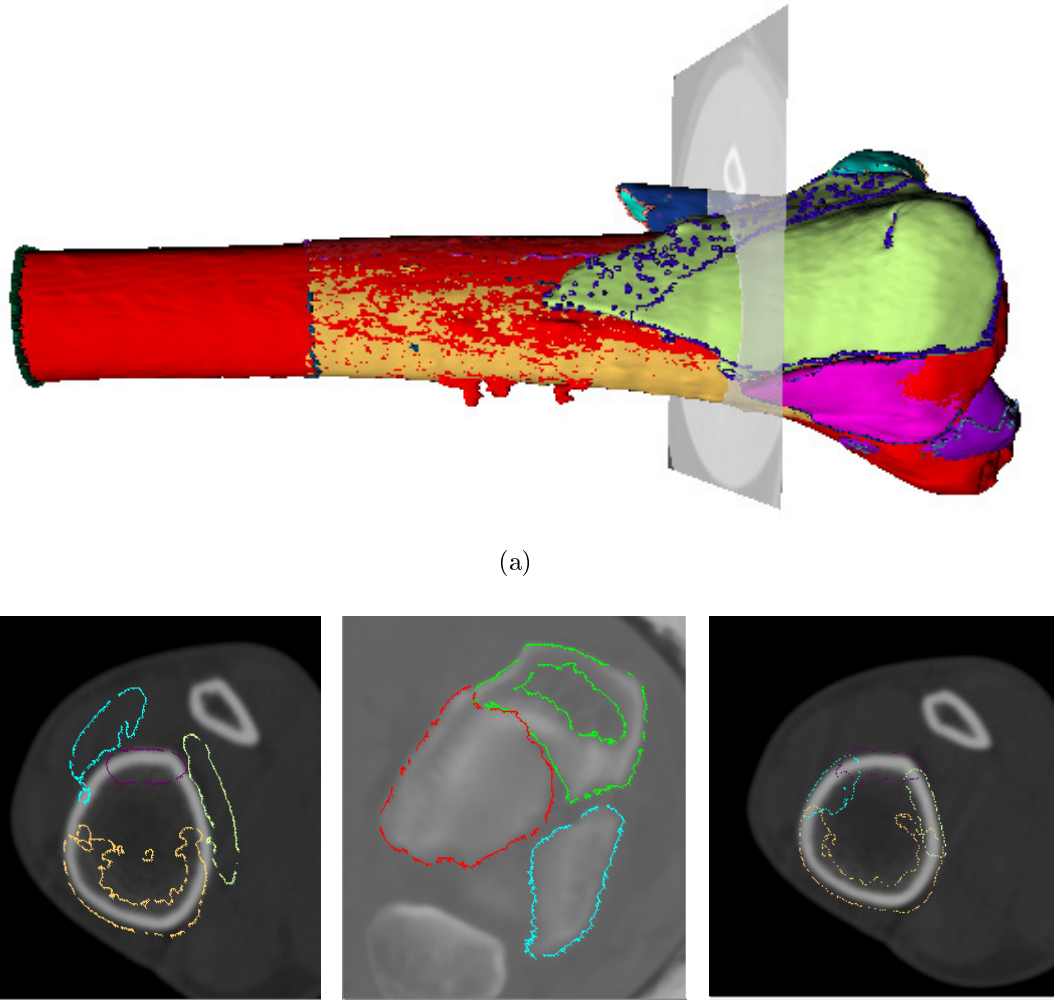

(a)

(b) (c) (d)

Figure 5.6: Case 11: Correlation compuation and evaluation (a) shows a 3d visualization of the misaligned fragments in case 11. (b) shows misaligned fragments' contour inscribed in its intact template in DICOM. The fracture contours appear away from the intact bone suggesting significant fracture displacement. (c) shows misaligned fragments' contour inscribed in its fracture DICOM image. The contours of fracture fragments coincide with the fracture contours in DICOM suggesting acceptable amount of accuracy in the inscription process. (d) shows fracture fragments' location of 3d reconstructed model inscribed in an intact DICOM template.

'Before Align' in correlation between Figure 5.6(b) and Figure 5.6(c), i.e., intensities of misaligned fracture point position in intact and fracture DICOM. 'After align' lists correlation between Figure 5.6(c) and Figure 5.6(d).

5.6.5 Analysis

The correlation numbers display a very good quality of virtual reconstruction of the fractured bone since maximum correlation value increase is ~0.80. With large translational and angular displacement, this case suggests a high force trauma. Although, with almost 80% accurate reconstruction and very minimal articular damage, with large number of fragments and dominant cortical damage this fracture case can be considered as severe .

5.7 Case 12: All-Terrain Vehicle Accident

5.7.1 Feature 1 and 2: Total Translational And Angular Displacement Measure

Figure 5.7(b) and Figure 5.7(d) gives a graphical reference to view the fragment translational displacement in intact space. As observed from the following table, frag5 undergoes low translational and high angular displacement suggesting localized rotational displacement.

Table 5.25: Case 12: Fracture fragment-based translational and angular displacement values with the translational and angular fracture feature values indicated in bold.

Frag #	Translational measure (mm)	$\alpha(^o)$	$\beta(^o)$	$\gamma(^o)$	Total angular displacement (^{o})
Frag 1	0	0	0	0	0
Frag 2	6.14	10.44	12.92	12.61	35.97
Frag 3	3.37	5.64	14.74	13.63	34.01
Frag 4	4.30	3.78	4.13	5.44	13.35
Frag 5	1.9	67.03	42.79	80.35	190.17
	15.71	86.89	74.58	112.03	**273.5**

5.7.2 Feature 3: Skewness Of Fracture Surface Intensity Profile

The statistical data obtained from all the fragments in this case is tabulated in Table 5.26. The skewness value suggests a dominant cancellous bone presence along the fracture surface.

Table 5.26: Case 12: Key parameters of the fracture surface intensity distribution including skewness and other statistical data for fracture surface intensity profile. The skewness fracture feature value is shown in bold.

Frag #	mean	median	mode	skewness	std	var
Frag 1	-1.0905e+03	-1137	-1024	2.4210	235.5147	5.5467e+04
Frag 2	-1.0430e+03	-1099	-1024	1.9982	298.7278	8.9238e+04
Frag 3	-1.2687e+03	-1293	-1399	1.0533	133.9976	1.7955e+04
Frag 4	-812.7879	-937	-1024	1.5247	317.0797	1.0054e+05
Frag 5	-1.1633e+03	-1148	-1216	-0.2663	132.5000	1.7556e+04
Average				**1.3**		

5.7.3 Feature 4 and 5: Total Fracture Surface Area (FSA) And Total Fracture Surface Perimeter (FSP)

Table 5.27 tabulates FSA and FSP values for all the fragments involved in this case.

Table 5.27: Case 12: Fracture surface area and surface perimeter features are computed for each fracture fragment. These valeus are summed to generate the case FSA and FSP fracture feature values which are shown in bold.

Frag #	FSA	Articular Area	Total FSA	FSP	Articular perimeter
Frag 1	6484.86	158.90	6643.76	14269.45	857.08
Frag 2	1478.39	207.20	1685.59	9694.12	1108.41
Frag 3	1244.11	173.46	1417.57	6574.93	737.02
Frag 4	575.31	-	575.31	3212.02	-
Frag 5	164.05	-	164.05	981.29	-
	9946.72	539.56	**10486.28**	**34731.81**	2702.51

5.7.4 Correlation: Accuracy Of Reconstruction Measure

From Table 5.28 for case 12. As expected, an increase is seen in correlation, for all the fragments, after alignment. Better alignment indicates better reconstruction.

Table 5.28: Case 12: Correlation between the gray scale intensities at the fragment positions in the intact and fracture DICOM, before and after the alignment.

Case 12		Correlation	
Frag #	No. of surface points	Before align5.7 (b), (c)	After align5.7 (c), (d)
Frag 1	34751	0.57	0.57
Frag 2	9035	0.19	0.48
Frag 3	8491	0.46	0.29
Frag 4	2241	0.07	0.59
Frag 5	470	-0.08	0.04

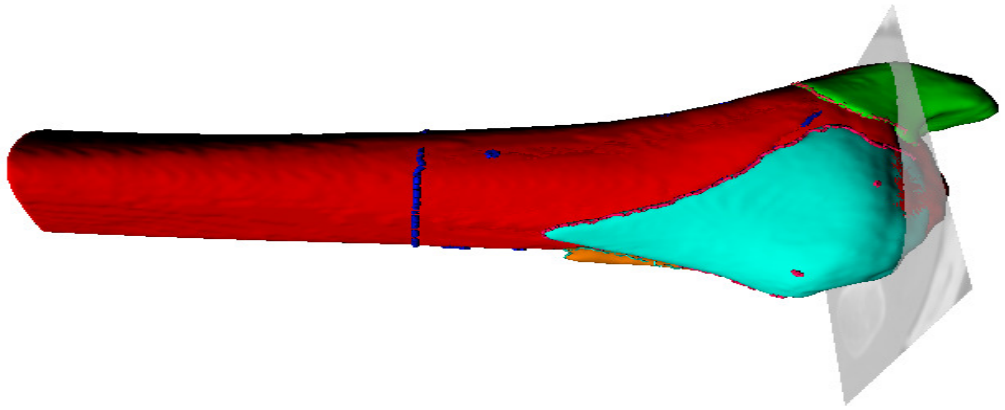

(a)

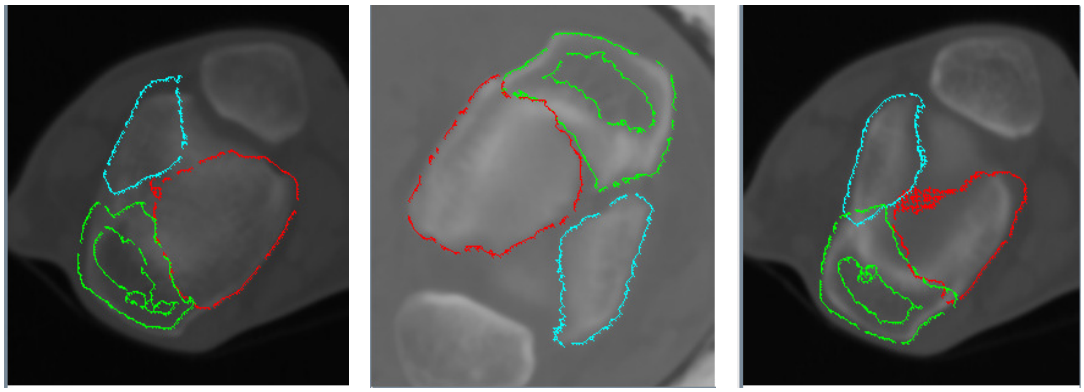

(b) (c) (d)

Figure 5.7: Case 12: Correlation computation and evaluation (a) shows a 3d visualization of the misaligned fragments. (b) shows misaligned fragments' contour inscribed in its intact template in DICOM. The fracture contours appear away from the intact bone suggesting significant fracture displacement. (c) shows misaligned fragments' contour inscribed in its fracture DICOM image. The contours of fracture fragments coincide with the fracture contours in DICOM suggesting acceptable amount of accuracy in the inscription process. (d) shows fracture fragments' location of 3d reconstructed model inscribed in an intact DICOM template.

5.7.5 Analysis

The correlation numbers display a average quality of virtual reconstruction of the fractured bone since maximum correlation value increase is ~0.60. With average translational and angular displacement this case suggests a average force trauma. Overall, with almost 60% accurate reconstruction and very minimal articular damage, this fracture case can be considered as medium severe.

5.8 Cases And Feature Values

Following table lists various features and their values obtained for every case.

Table 5.29: Condensed matrix where, α, β, γ are angular displacements; FSA is surface area; FSP is surface perimeter; Art% is articular percentage in the fracture; Corr is correlation; Trans is translational motion; skewness is the intensity histogram skewness; N is number of fragments.

Case	**Angle**	**FSA**	**FSP**	Art%	Corr	**Trans**	**Skewness**	N
6	**765.4**	**8962.11**	**48189**	13	0.48	**83.09**	**0.73**	10
7	**963.4**	**6948.79**	**62701**	10	0.50	**63.12**	**0.87**	6
8	**752.23**	**8827.75**	**57145**	10	0.26	**70.45**	**0.99**	6
9	**69.49**	**3467.59**	**46624**	24	0.76	**7.72**	**0.97**	3
10	**138.1**	**18870.92**	**82792**	4	0.51	**10.01**	**0.95**	4
11	**362.5**	**2544.67**	**156108**	3	0.62	**52.27**	**-0.06**	8
12	**273.5**	**10486.28**	**37433**	5	0.39	**15.71**	**1.13**	5

This thesis uses the fracture feature values extracted above (in bold) and evaluates them based on their performance when used to predict the clinical fracture severityeach of these fracture cases.

CHAPTER 6: FRACTURE SEVERITY PREDICTIVE PERFORMANCE FOR SELECTED FRACTURES

This chapter evaluates the performance of the five selected fracture feature values for predicting fracture severity. The values of these features were extracted from 3D CT image data of seven clinical fracture cases using a computational fracture reconstruction system and several custom built functions to tabulate the specific features of interest. Here, the performance of these features for the purpose of predicting fracture severity is analyzed by comparing the feature values against KL-scores and overall severity values assigned to these cases by practicing orthopaedic surgeons [57].

6.1 Linear Regression Analysis

Linear regression hypothesizes that a linear relationship exists between a scalar dependent variable, Y, and a second explanatory variable, X. Analysis is done by performing linear regression, i.e., computing a linear fit between the X and Y values under the assumption that these values are related by the equation $Y = mX+b$, where both the slope of the line, m, and the $Y - axis$ intercept b are unknown. For performance analysis, the Y values are taken as severity scores assigned by orthopaedic surgeons and X values are taken as the values of a fracture feature. Estimates for the unknowns m and b are obtained by computing the least-squares fit between the (X, Y) data points as indicated in equation [4.2] where $alpha = [m,\ b]^t$, $Y = \begin{bmatrix} Y_0 \\ Y_1 \\ \vdots \\ Y_{N-1} \end{bmatrix}$ and

$M = \begin{bmatrix} X_0 & 1 \\ X_1 & 1 \\ \vdots & \vdots \\ X_{N-1} & 1 \end{bmatrix}$ for a set of N (X, Y) pairs of measured data. The error is taken as the absolute difference between the measured Y values and the Y values that lie on the best-fit line as indicated in 6.2.

$$\alpha = inv(M^t * M) * M^t * Y) \tag{6.1}$$

$$absError = abs(Y^t - M * \alpha) \tag{6.2}$$

6.2 Total Fracture Fragment Translational And Orientation Change Measure

The displacement of every fragment in each case is studied and total translation and total orientation in (α, β, γ) are taken as parameters to independently predict fracture severity for every case. Linear fit error is computed with respect to overall severity and KL score for all the cases.

Table 6.1: Best-fit error computation for total translation and total orientation features for all fractures cases.

Case #	Total Translational	Total Orientation	Linear Best-Fit Error (Translation Vs Savg)	Linear Best-Fit Error (Translation Vs KL)	Linear Best-Fit Error (Orientation Vs Savg)	Linear Best-Fit Error (Orientation Vs KL)
6	83.09	1401.7	12.9	1.8	9	0.8
7	63.12	962.4	4.4	0.8	2.2	0.9
8	70.45	751.3	9.7	0.6	19.9	1.3
9	7.72	69.5	13.39	1.2	22.2	1.9
10	10.01	138.1	26.4	1.7	17.3	0.2
11	52.27	273.7	16.2	1.2	26.6	0.8
12	15.71	272.8	21.5	1.4	30.3	2.6
Total			104.4	8.0	127.3	8.5

Table 6.2: Correlation coefficient (R) comparison between displacement parameters and average overall ranking and KL score.

R	Overall severity	KL-score
Translation	0.68	0.28
Orientation	0.55	0.25

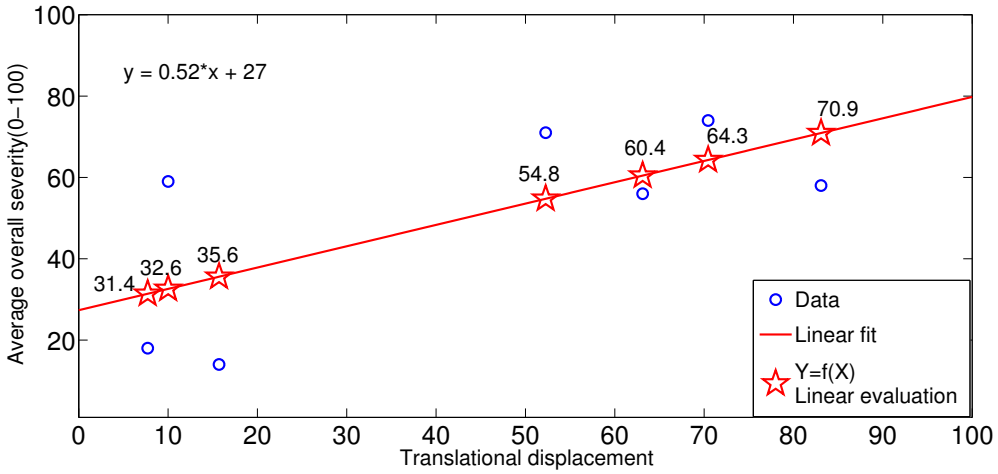

(a) Graph for total translation Vs Savg-Linear fit

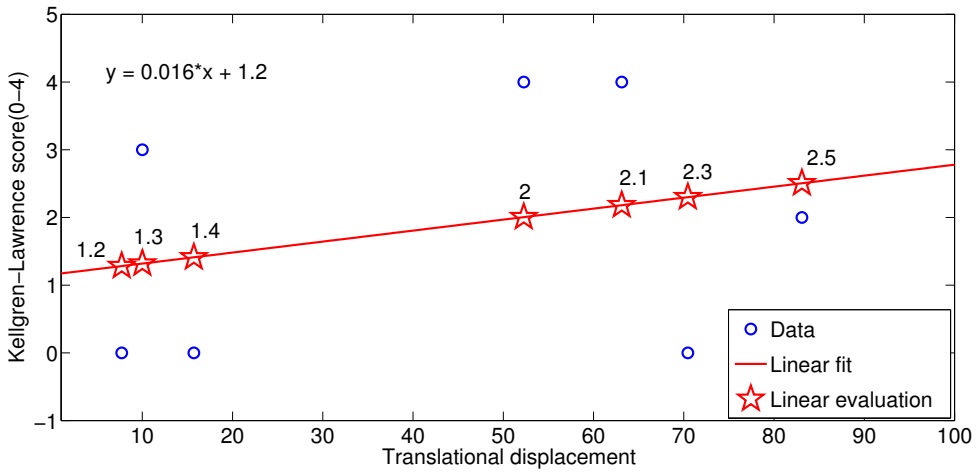

(b) Graph for total translation Vs KL-Linear fit

Figure 6.1: Linear fitting translational displacement to average overall severity (Savg) and KL score.

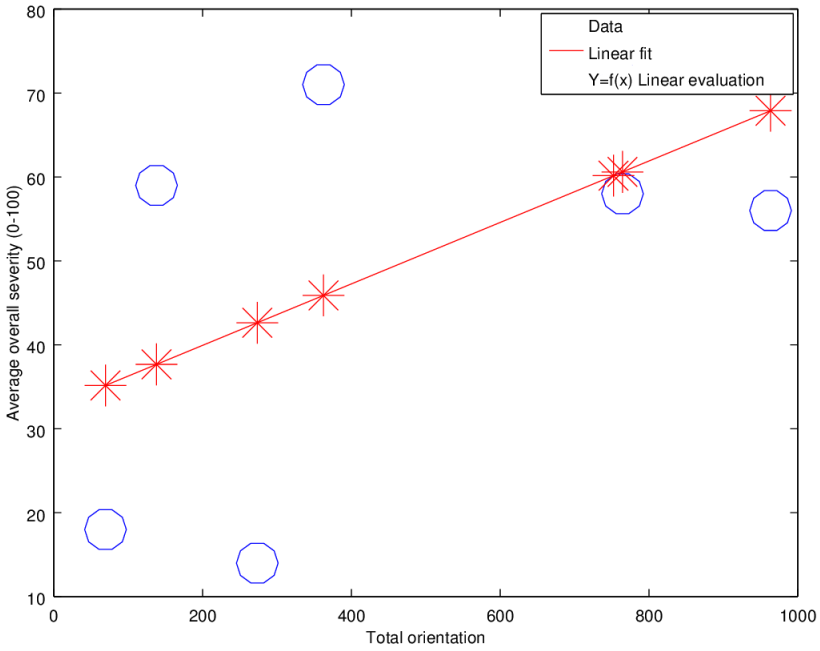

(a) Graph for total orientationVs Savg-Linear fit.

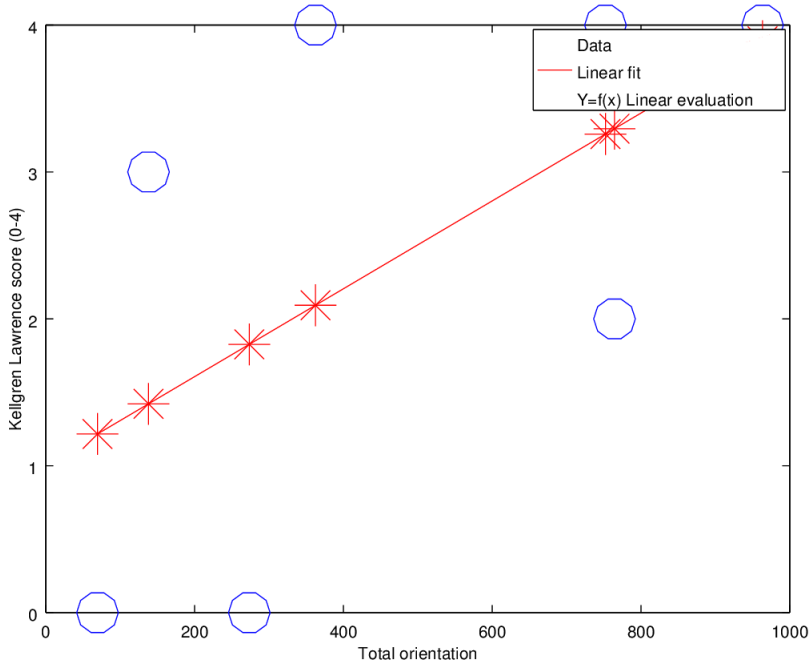

(b) Graph for total orientationVs KL-Linear fit.

Figure 6.2: Linear fitting total orientation to average overall severity (Savg) and KL score.

6.3 Skewness Of Fracture Surface Intensity Profile

Histogram of intensity values of a virtually reconstructed fracture surface are plotted in intact space and different statistics like mean, median, mode, skewness and standard deviation are calculated Table 6.2a. The histograms are computed for every fragment of the case and then averaged to obtain a single value. Out of these statistical parameters skewness is taken as an indicator of the extent of fracture severity.

Table 6.3: Fracture measure: Skewness.

(a) Best fit error computation of skewness values for all the cases.

Case #	mean	median	mode	skewness	std	Skewness Best-Fit Error (Savg)	Skewness Best-Fit Error (KL)
6	-1059	-1102	-1121	0.738	291.2	10.8	0.38
7	-1346	-1351	-1335	0.87	194	1.38	1.5
8	-940	-982	-1031	0.995	370	17.88	1.6
9	-1381	-1430	-1539	0.97	285	32.8	2.4
10	-615	-799	-1021	0.95	478	11.4	0.54
11	-288	-264	-280	-0.06	236	25.11	1.5
12	-1075	-1122	-1137	1.308	223	33.8	2.4
Total						132.6	10.2

(b) Correlation coefficient comparison between the skewness and overall severity and KL score.

R	Overall severity	KL score
Skewness	-0.52	-0.63

Skewness values listed in Table 6.2a are correlated with their KL-score and overall

severity values and result is in Table 6.2b. Negative correlation values in Table 6.2b reveal that the negative skew value is an indication of higher severity. Negative skewness indicates presence of large number of fracture points in the denser region or the cortical region. A fracture that causes damage to the denser bone can be considered as severe due to the account of the high energy involved in breaking apart a denser bone. As perceived, the fracture to cortical bone indicates high intensity fracture Table 6.3b.

This observation is also validated by observing linear fit polynomial between scores and skewness values as shown in Figure 6.3. The inverse relation in the graphs indicate that negative skewness evaluates to higher severity.

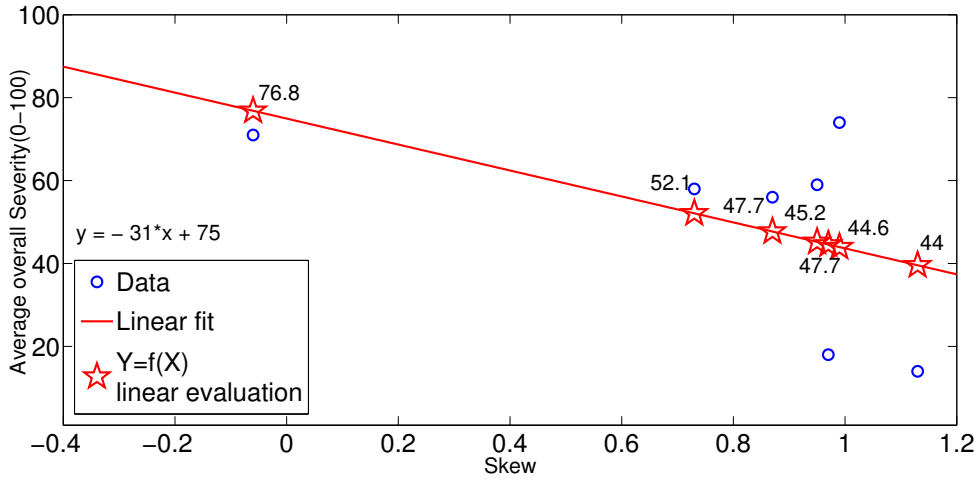

(a) Skew Vs Savg-Linear fit

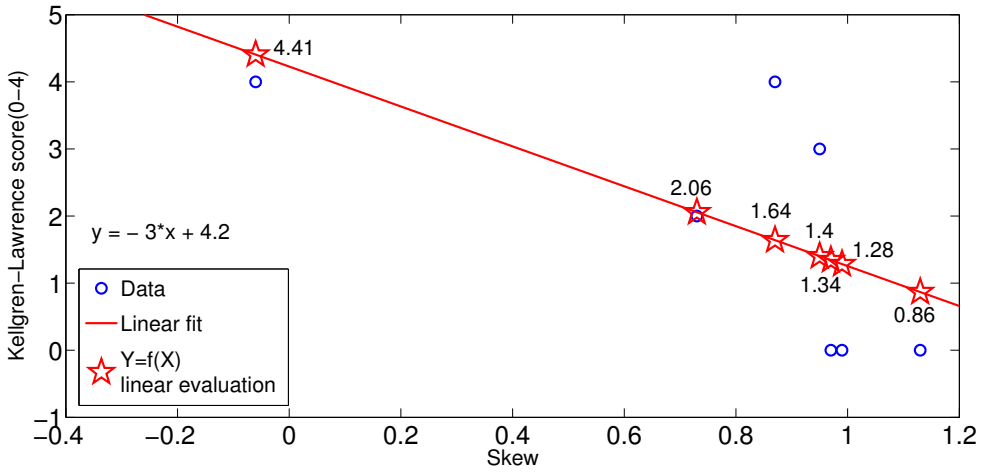

(b) Skew Vs KL-Linear fit

Figure 6.3: Linear fitting skew values to KL and Average overall severity.

This stresses on the fact that severity mostly depends on the cortical damage than cancellous bone.

6.4 Total Fracture Surface Area And Total Fracture Surface Perimeter

The fracture surface area for every fragment in the case is computed and then added to get a total fracture surface area value. Conceptually, fracture surface area is expected to be a predictor of fracture severity because the surface area generated by the fracture is directly proportional to the force responsible for the fracture. Larger

force result in larger fracture surface hence higher severity. Similar logic applies for fracture surface perimeter computation.

Table 6.4: Total FSA and FSP.

(a) Total FSA and FSP for all fracture cases.

Case #	FSA	FSP	Best-Fit Error (FSA Vs Savg)	Best-Fit Error (FSA Vs KL)	Best-Fit Error (FSP Vs Savg)	Best-Fit Error (FSP Vs KL)
6	8962	41876	12.4	0.32	15.6	0.42
7	6948	58242	13.7	0.41	8.1	1.2
8	8827	50832	28.6	2.02	28.6	2.33
9	3467	40997	18.5	1.1	24.0	2.18
10	18870	77743	2.9	1.00	4.6	0.80
11	23968	149168	0.69	0.39	7.1	0.27
12	10486	34731	34.0	2.2	25.9	2.0
Total			110.79	7.3	113.9	9.0

(b) Correlation coefficient (R) comparison between fracture surface parameters and average overall severity and KL score.

R	Overall severity	KL-score
FSA	0.49	0.59
FSP	0.56	0.68

Fracture surface area (FSA) and fracture surface perimeter (FSP) act as an independent measure for predicting fracture severity. The direct relation in the following graphs indicate that higher FSA and FSP evaluates to higher fracture severity.

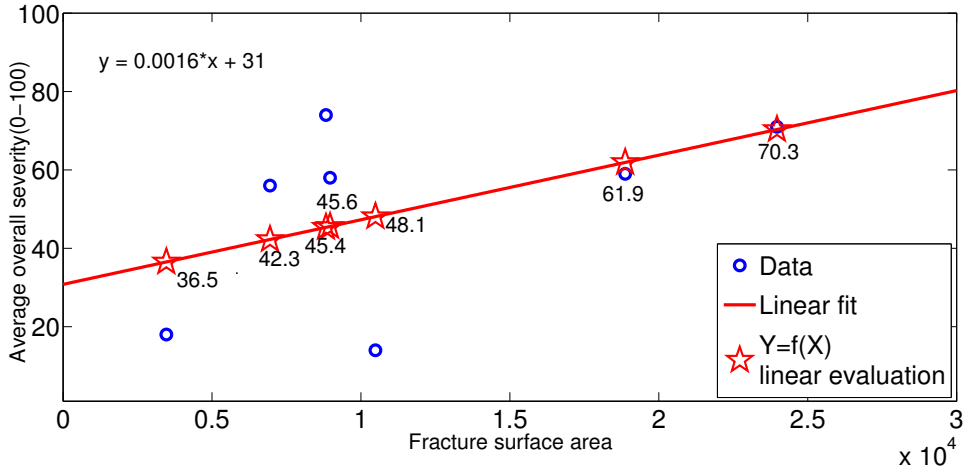

(a) FSA Vs Savg-Linear fit.

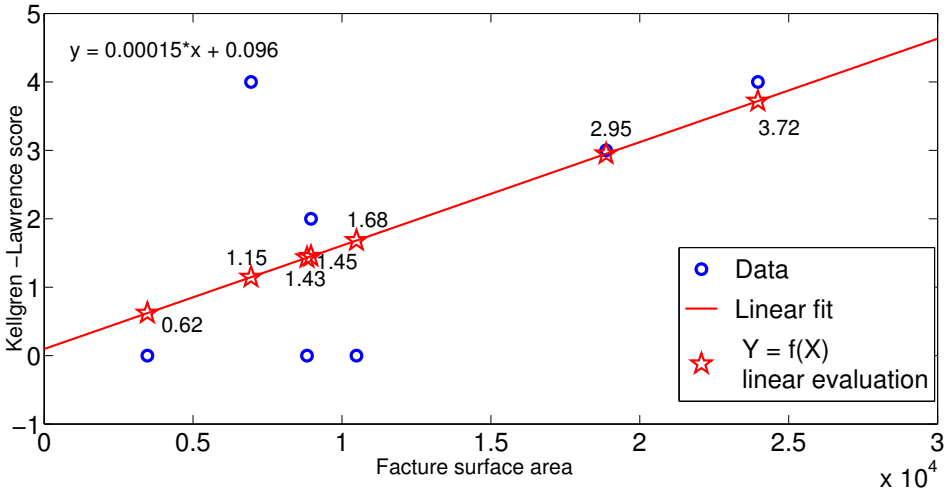

(b) FSA Vs KL score-Linear fit.

Figure 6.4: Linear fitting fracture surface area to KL and Average overall severity.

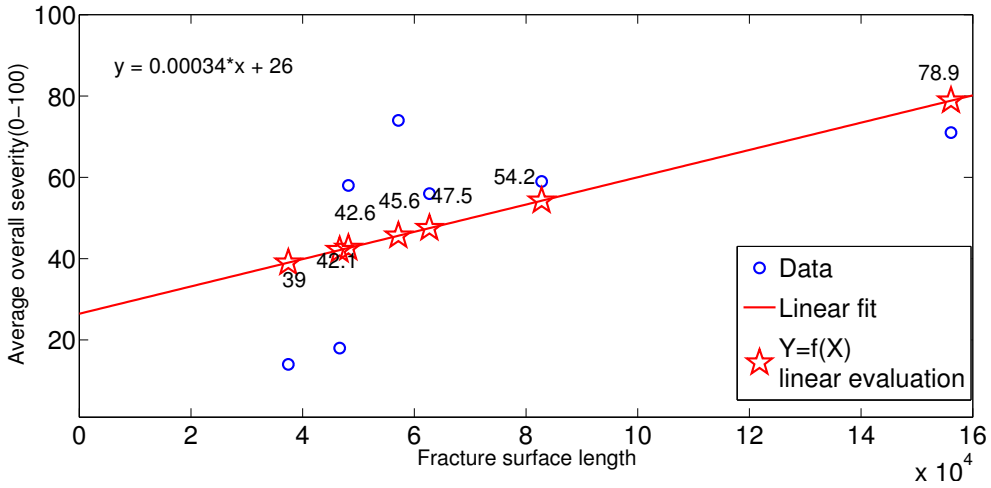

(a) FSP Vs Savg-Linear fit.

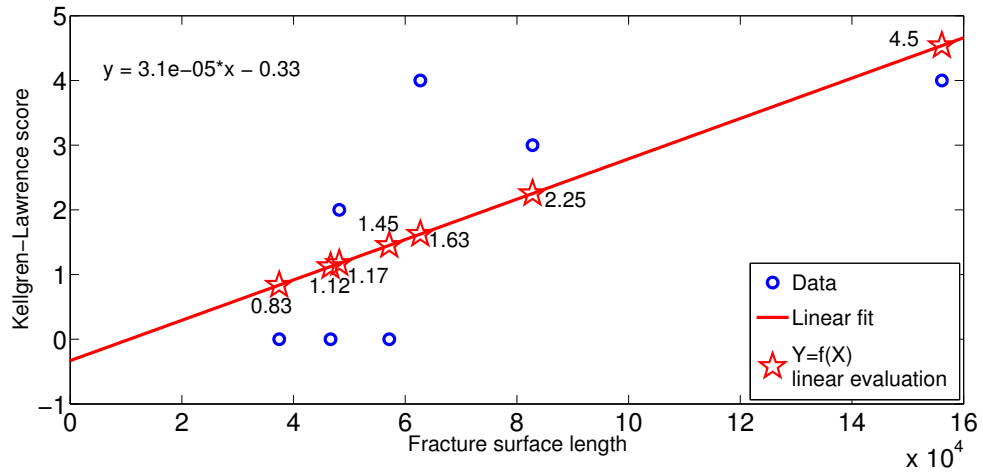

(b) FSP Vs KL score-Linear fit.

Figure 6.5: Linear fitting fracture surface length to KL and Average overall severity.

6.5 Best-Fit Error Analysis

For each fracture feature, the best-fit error is taken as the total error observed between the best-fit line and the fracture severity values assigned to each case by the orthopaedic surgeons. Low total error indicates that a feature is a better predictor of the fracture severity assigned by the orthopaedic surgeons. Feature values are plotted against clinically-assigned fracture severity scores and linear fit that hypothesizes a linear correlation between the computed feature values and the clinically-assigned

fracture severity scores. The slope of the fit line indicates whether the feature is positively or negatively correlated to the clinically-assigned feature values. Apart from skewness, all other features bear a positive correlation to clinically-assigned severity scores. Using this metric, the translational displacement fracture feature shows the least total fit error.

6.6 Correlation

The correlation obtained between the intensities of aligned fracture fragments in the intact and the fracture DICOM templates is used as a measure of reconstruction accuracy. For each case, the correlation of intensity values between the intact bone intensities and the reconstructed bone fragment intensities is computed as a measure of reconstruction accuracy for that case. The correlation is computed for each fragment and then averaged over all fragments as indicated in (6.3) below

$$R_{avg} = \frac{\sum_{i=1}^{N} \rho_{\mathrm{i}}}{N} \tag{6.3}$$

where N denotes number of fracture fragments and ρ_i denotes correlation value of a fragment in a fracture case, value of i goes from 1 to N. For this measure, higher values indicate that the reconstruction solution includes a better alignment of the bone fracture fragments. Better alignment imply better reconstruction and thus correlation values are positive as shown in equation [6.3] Table 6.4a. Complex fractures have larger reconstruction error and are prone to having less accurate fracture feature values. Cases 6, 8 and 12 show lower correlation values indicating that their reconstruction may be less accurate than other reconstructions. Table 5.29 shows that cases 6, 8 and 12 are all severe fractures with high translation, FSA and FSP feature values. These cases also have a large number of fragments which make reconstruction more complex and indicates that the quality of the reconstruction degrades for more severe fractures.

Table 6.5: Correlation comparison between the gray scale intensities at the fragment positions in the intact and fracture DICOM, after the alignment.

(a) Average correlation.

Case #	6	7	8	9	10	11	12
Correlation in aligned position of fragments	0.48	0.50	0.29	0.76	0.51	0.62	0.39

(b) Correlation coefficient comparison: correlation vs overall severity/ KL score.

	Overall severity (Savg)	KL score (KL)
R (correlation)	-0.33	-0.24
R $>$ 0.50	-0.71	-0.63

Correlation values are correlated with their KL-score and overall severity values Table 6.4b. As shown, correlation is inversely proportional to severity scores. Thus, higher correlation value suggests better reconstruction and lower fracture feature values; lower fracture feature values imply lower fracture severity.

6.7 Summary

Sections 6.2 - 6.4 elaborate on the best fit errors computed for all five fracture features. For every feature the error (or disturbance) of an observed value is the deviation of the observed value from the true function value (linear equation). This statistical error is based of the entire population of the data set, i.e, the fracture values considered for computing linear error.

CHAPTER 7: CONCLUSION

This thesis proposes five new fracture features and provides an initial analysis that indicates the performance of these features for automatic fracture severity assessment. Linear best-fit errors are computed between the computed feature values and severity assessment values provided by orthopaedic surgeons for seven clinical fracture cases. The performance score for each fracture feature is taken as the total error observed between the best-fit regression model and the fracture severity values assigned to each case by the surgeons. For the fracture features analyzed and the performance metric adopted the translational displacement fracture feature was found to have the highest predictive performance.

REFERENCES

[1] T. Thomas, D. Anderson, L. Marsh, and T. Brown, "Displaced soft tissue volume as a metric of comminuted fracture severity," *Annual Meeting of the American Society of Biomechanics*, pp. 22–25, 2007.

[2] C. Beardsley, D. Anderson, L. Marsh, and T. Brown, "Inter fragmentary surface area as an index of comminution severity in cortical bone impact," *Journal of Orthopaedic Research*, vol. 23, pp. 680–690, 2005.

[3] J. Marsh, J. Buckwalter, and R. Gelberman, "Articular fractures: Does an anatomic reduction really change the result?," *The Journal of Bone and Joint Surgery*, vol. 84, pp. 1259–1271, 2002.

[4] C. Charalambous, M. Tryfonidis, F. Alvi, M. Moran, C. Fang, R. Samaraji, and P. Hirst, "Inter- and intra-observer variation of the schatzker and AO OTA classifications of tibial plateau fractures and a proposal of a new classification system," *The Journal of Bone and Joint Surgery*, vol. 84, pp. 1259–1271, 2002.

[5] B. Joseph and B. Thomas, "Joint injury, repair, and remodeling: roles in post-traumatic osteoarthritis," *Clinical Orthopaedics and Related Research*, vol. 423, pp. 7–16, 2004.

[6] R. Brumback and A. Jones, "Interobserver agreement in the classification of open fractures of the tibia the results of a survey of two hundred and forty five orthopaedic surgeons," *The Journal of Bone and Joint Surgery*, vol. 76, pp. 1162–1166, 1994.

[7] B. JA, "Sports, joint injury, and posttraumatic osteoarthritis," *J Orthop Sports Phys Ther*, vol. 33, pp. 78–88, 2003.

[8] P. Conaghan and L. Sharma, "Fast facts: Osteoarthritis," 2009.

[9] P. Liu, "A system for computational analysis and reconstruction of 3d comminuted bone fractures," 2012.

[10] J. Rogowska1 and M. E. Brezinski, "Image processing techniques for noise removal, enhancement and segmentation of cartilage OCT images," *Physics in medicine and biology*, vol. 47, 2002.

[11] K. JH and L. JS, "Radiological assessment of osteo-arthrosis," *Annals of the Rheumatic disease*, vol. 4, pp. 494–502, 1957.

[12] T. E. S. Foundation, "Medical imaging for improved patient care," 2007.

[13] M. P, E. M, and M. E, "Introduction to the DICOM standard," *European radiology*, vol. 4, pp. 920–7, 2002.

[14] A. Rosset, L. Spadola, and O. Ratib, "Osirix: An open-source software for navigating in multidimensional DICOM images," 2004.

[15] "Digital imaging and communications in medicine DICOM," *National Electrical Manufacturers Association*, 2009.

[16] A. Willis, D. Anderson, T. Thomas, Brown, and J. Marsh, "3d reconstruction of highly fragmented bone fractures," *Proceedings of the SPIE Conference on Medical Imaging 2007: Image Processing*, vol. 6512, pp. 1–10, 2007.

[17] "Anatomy of an ankle." http://www.gla.ac.uk/ibls/US/fab/tutorial n/anatomy/anklet.html.

[18] D. G. N, E. Miriam, L. Lawrence, H. Jan, K. Max, and S. Klaus, "Chondrocyte death precedes structural damage in blunt impact trauma," *Clinical Orthopaedics & Related Research*, vol. 393, pp. 302–309, 2001.

[19] S. V, A. D, G. H, G. C, E. KH, and R. M. andEckstein F, "Correlation of cartilage quantity between the knee and ankle in normal volunteers and in monozygotic twins," *Institute of Anatomy-Musculoskeletal Research Group.*

[20] "Types of fracture." http://www.medicinenet.com/fracture/article.htm.

[21] D. Ovadia and R. Beals, "Fractures of the tibial plafond," *The Journal of Bone and Joint Surgery*, vol. 68, pp. 543–551, 1986.

[22] "Oa commonly affected joints." http://www.spineuniverse.com/conditions n/spondylosis/osteoarthritis-commonly-affected-joints.

[23] R. EL and R. RM, "Role of subchondral bone in the initiation and progression of cartilage damage," *UK PubMed Central*, vol. 213, pp. 34–40, 1986.

[24] H. Kirchner, "Ductility and brittleness of bone," *International Journal of Fracture*, vol. 139, pp. 509–516, 2006.

[25] D. Douglas and D. Patrick, "Injury severity assessment in tibial plateau fractures," *Clinical Orthopaedics & Related Research*, vol. 423, pp. 85–92, 2004.

[26] van den Bekerom, H. D, and K. P, "Biomechanical and clinical evaluation of posterior malleolar fractures. a systematic review of the literature.," *Journal of Orthopaedic Trauma*, vol. 66, pp. 279–84, 2009.

[27] S. CL, Z. MB, R. M, B. TD, B. JA, and J. R, "Impact of comorbidities on the measurement of health in patients with ankle osteoarthritis," *The Journal of Bone and Joint Surgery*, vol. 88, pp. 2366–72, 2006.

[28] B. TD, J. RC, S. CL, M. JL, and B. JA, "Posttraumatic osteoarthritis: a first estimate of incidence, prevalence, and burden of disease," *J Orthop Trauma*, vol. 20, pp. 739–44, 2006.

[29] B. J and W. Ricci, "Acute effects of cartilage impact," *Clinical Orthopaedics and Related Research*, vol. 423, pp. 33–39, 2004.

[30] O. S. A and G. Farshid, "From articular fracture to posttraumatic arthritis: A black box that needs to be opened," *Journal of Orthopaedic Trauma*, vol. 20, pp. 61–62, 2006.

[31] D. Roylance, "Introduction to fracture mechanics," *European Cells and Materials*, vol. 9, pp. 23–32, 2001.

[32] B. JC and B. W, "Fracture mechanics of bone–the effects of density, specimen thickness and crack velocity on longitudinal fracture," *The Journal of Biomechanics*, vol. 17, pp. 25–34, 1984.

[33] B. AL and P. AS, "Bone structure, composition and mineralization," *Pub med*, vol. 15, pp. 507–612, 1984.

[34] Y. YN, B. CU, and N. TL, "Influence of bone composition and apparent density on fracture toughness of the human femur and tibia," *Bone*, vol. 22, pp. 79–84, 1998.

[35] M. RJ, H. WC, E. WT, G. RP, and W. A. 3rd, "Prediction of vertebral body compressive fracture using quantitative computed tomography," *Bone*, vol. 67, pp. 1206–14, 1985.

[36] A. Gefen, "Bone structure and composition," *Lecture*.

[37] L. Gibson, "Biomechanics of cellular solids," *Journal of Biomechanics*, vol. 38, pp. 377–399, 2004.

[38] Y. Y, Z. X, A. D, B. T, H. Van, and S. M, "Simultaneous segmentation of the bone and cartilage surfaces of a knee joint in 3d," *Proceedings of the SPIE on Medical Imaging*, vol. 7258, pp. 1–9, 2009.

[39] K. PakinQ, R. Gaborski, L. Barskic, D. Foosd, and K. Parkere, "Segmentation of bone and soft tissue regions in digital,"

[40] D. Anderson, V. Muehling, J. Marsh, and T. Brown, "Precise identification of bone fragment boundaries to assist in reduction of highly comminuted bone fractures," *Computer Aided Surgery*, vol. 9, p. 116, 2004.

[41] S.-Y. Chien, Y.-W. Huang, and L.-G. Chen, "Predictive watershed: a fast watershed algorithm for video segmentation," *Circuits and Systems for Video Technology, IEEE Transactions*, vol. 13, pp. 453–461, 2003.

[42] M. A.P and W. R.T, "Partitioning 3d surface meshes using watershed segmentation," *Visualization and Computer Graphics, IEEE Transactions*, vol. 5, pp. 308–321, 1999.

[43] A. Willis and B. Zhou, "Ridge walking for 3d surface segmentation," *University of North Carolina*, 2010.

[44] R. Adams and L. Bischof, "Seeded region growing," *Pattern Analysis and Machine Intelligence, IEEE Transactions*, vol. 16, pp. 641–647, 1994.

[45] Y. Lua, T. Jiang, and Y. Zanga, "Region growing method for the analysis of functional mri data," *NeuroImage*, vol. 20, pp. 455–465, 2003.

[46] O. Ron, L. Joskowicz, A. Simkin, and C. Milgrom, "Computer-based periaxial rotation measurement for aligning fractured femur fragments: methods and preliminary results," *Lecture Notes in Computer Science*, vol. 2208, pp. 17–23, 2001.

[47] C. L, B. F. Bernardini, and G. Xu, "Reconstruction of surfaces and surfaces-on-surfaces from unorganized weighted points," *Computer Science Technical Report CSD*, 1994.

[48] M. Scheuering, C. Rezk-Salama, C. Eckstein, and G. Hormann, "Interactive repositioning of bone fracture segments," *Proceedings of Vision, Modeling and Visualization (VMV)*, pp. 499–505, 2001.

[49] M. Harders, A. Barlit, C. Gerber, J. Hodler, and G. Szekely, "An optimized surgical planning environment for complex proximal humerus fractures," *MICCAI Workshop on Interaction in Medical Image Analysis and Visualization*, pp. 1–8, 2007.

[50] N. Amenta, M. Bern, and M. Kamvysselisy, "A new voronoi-based surface reconstruction algorithm," in *SIGGRAPH: Proceedings of the 25th annual conference on Computer graphics and interactive techniques*, 1999.

[51] P. Alfeld, "Scattered data interpolation in three or more variables," *Mathematical methods in computer aided geometric design*, pp. 1–34, 1989.

[52] B. Zhou, Y. Sui, and A. Willis, "Improving inter-fragmentary alignment for virtual 3d reconstruction of highly fragmented bone fracture," *Proceedings of the SPIE on Medical Imaging*, vol. 7528, pp. 1–9, 2009.

[53] K. Tipirneni, "Fracture classification and description," *Lecture presentation.*

[54] G. Rounds and M. Orthopaedics, "Distal tibial fractures," 2007.

[55] K. J.H and J. Lawrence, "Relations of mechanical properties to density and CT numbers in human bone," *Ann Rheum Dis*, vol. 16, pp. 594–502, 1957.

[56] I. F. Petersson, T. Boegard, T. Saxne, A. J. Silman, and B. Svensson, "Radiographic osteoarthritis of the knee classified by the ahlback and kellgren and lawrence systems for the tibiofemoral joint in people aged 35 to 54 years with chronic knee pain," *Annals of the Rheumatic Diseases*, vol. 28, pp. 493–496, 1997.

[57] D. D.R. and S. Ferry, "Reliability of classification of fractures of the tibial plafond according to a rank-order method," *J Trauma*, vol. 61, pp. 1463–6, 2006.